



# New low mass ratio contact binaries in the Catalina Sky Survey

Panagiota-Eleftheria Christopoulou<sup>1</sup>, Eleni Lalounta<sup>1</sup>, Athanasios Papageorgiou<sup>1</sup>, C. E. Ferreira Lopes<sup>2</sup>, Márcio Catelan<sup>3,4,5</sup> and Andrew J. Drake<sup>6</sup>

<sup>1</sup>Department of Physics, University of Patras, 26500 Patra, Greece

<sup>2</sup>Astrophysics Division, National Institute for Space Research (DAS/INPE), Av. dos Astronautas, 1758 - Jardim da Granja, São José dos Campos, SP 12227-010, Brazil

<sup>3</sup>Instituto de Astrofísica, Facultad de Física, Pontificia Universidad Católica de Chile, Av. Vicuña Mackenna 4860, 7820436 Macul, Santiago, Chile

<sup>4</sup>Millennium Institute of Astrophysics, Nuncio Monseñor Sotero Sanz 100, Of. 104, Providencia, Santiago, Chile

<sup>5</sup>Centro de Astroingeniería, Pontificia Universidad Católica de Chile, Av. Vicuña Mackenna 4860, 7820436 Macul, Santiago, Chile

<sup>6</sup>California Institute of Technology, 1200 East California, Boulevard, CA 91225, USA

Accepted 2022 February 22. Received 2022 February 22; in original form 2021 December 20

## ABSTRACT

We present the identification and photometric analysis of 30 new low mass ratio (LMR) totally eclipsing contact binaries found in Catalina Sky Survey data. The LMR candidates are identified using Fourier coefficients and visual inspection. We perform a detailed scan in the parameter plane of mass ratio ( $q$ ) versus inclination ( $i$ ) using PHOEBE -0.31 scripter to derive the best ( $q$ ,  $i$ ) pair for the initial models. The relative physical parameters are determined from the final model of each system. A Monte Carlo approach was adopted to derive the parameter errors. The resulting parameters confirm the identification. The approximate absolute physical parameters of the systems are estimated based on the light-curve solutions and *Gaia* Early Data Release 3 distances. 12 out of 30 new systems have fill-out factors  $f > 50$  per cent and  $q \leq 0.25$  (deep contact LMR systems), and eight of them, to within errors, are extreme LMR deep systems with  $q \leq 0.1$ . We discuss the evolutionary status of the 30 LMR systems in comparison with the most updated catalogue of LMR systems from the literature. The scenario of the LMR systems as pre-merger candidates forming fast rotating stars is investigated for all systems, new and old, based both on Hut's stability criteria and critical instability mass ratio ( $q_{\text{inst}}$ ) relation. CSS\_J075848.2+125656, with  $q/q_{\text{inst}} = 1.23 \pm 0.23$ , and CSS\_J093010.1–021624, with  $q/q_{\text{inst}} = 1.25 \pm 0.23$ , can be considered as merger candidates.

**Key words:** surveys – binaries: eclipsing – binaries: close – stars: evolution – stars: fundamental parameters.

## 1 INTRODUCTION

Eclipsing binary systems of EW light-curve type (EWs) with extreme low mass ratios challenge the current theoretical models since the latter predict coalescence into a single star (Robertson & Eggleton 1977; Eggleton 2010a, and references therein). In at least one case, V1309 Sco, such a merger event has been directly observed (Nakano et al. 2008). This defined a distinct new class of luminous red novae that was later attributed, upon analysis of archival photometric data from the Optical Gravitational Lensing Experiment (OGLE; Udalski 2003), to the merging components of a cool overcontact eclipsing binary system with a decreasing orbital period (Tylenda et al. 2011). What triggers the binary to merge is still controversial. The widely accepted scenario is Darwin's instability model (Darwin 1879), which implies that the merger happens when the spin angular momentum of the system is more than one-third of the orbital angular momentum (Hut 1980; Rasio 1995). When the binary mass ratio is extremely small and the secondary component has extremely small

mass, it can no longer continue to corotate synchronously with the primary via the tidal interaction. As a consequence of the secondary's higher angular velocity, angular momentum is transported rapidly from the orbital motion to the primary's spin, causing the orbit to shrink and the period to shorten, until the engulfment of the secondary. Models suggest that single stars (FK Com and blue straggler type) could be the result of this coalescence (Rasio 1995; Stępień 2006; Stępień & Kiraga 2015). In addition, both the loss of mass and angular momentum through magnetic winds (Stępień 2006, 2009; Stępień & Gazeas 2012) and the presence of other companion(s) play a crucial role in the merging process. Since most stars are in binaries, and a significant fraction are in triples or higher order systems (Tokovinin et al. 2006; Rucinski, Pribulla & van Kerkwijk 2007; Raghavan et al. 2010; Rappaport et al. 2013), potential stellar mergers may serve as keys to the binary fate. On the other hand, as orbital variations are common in contact binaries, the orbital period decay at a high rate induced by a third star proved to be crucial in the case of the recently claimed red nova precursor KIC 9832227 (Molnar et al. 2017) after the revision of its period variations (Socia et al. 2018; Kovacs, Hartman & Bakos 2019).

\* E-mail: [pechris@physics.upatras.gr](mailto:pechris@physics.upatras.gr)

Yang & Qian (2015) presented the first compilation of low mass ratio systems (LMRs) with high fill-out factor, and since then many systems have been detected (for reviews, see Qian et al. 2020; Gazeas et al. 2021b). Ongoing all-sky surveys have significantly increased the number of known systems with extreme low mass ratio (LMR), and many more will be discovered in the Rubin Observatory’s Legacy Survey of Space and Time (LSST) era (Ivezić et al. 2019).

This work focuses on the Catalina Sky Survey (CSS) and presents 30 new LMRs with total eclipses. In Section 2, we briefly describe the CSS sample and our method for identifying LMRs. In Section 3, we describe the photometric analysis of the CSS light curves (LCs) and the physical parameters determination. The methods for estimating the absolute parameters in absence of spectroscopic data are also discussed. Our results are presented in Section 4, where the possibility that they may be merger candidates is also discussed. Our final conclusions are summarized in Section 5.

## 2 SAMPLE SELECTION

### 2.1 The Catalina sample

Our sample is selected from the Catalina Real-Time Transient Survey Data Release 2 (CRTS DR2; Drake et al. 2014a), which includes observations spanning 9 yr (2004–2013). CRTS searches for optical transients by using the three CSS telescopes that search for rapidly moving near-Earth objects. CSS covers the sky between declinations  $\delta = -75^\circ$  to  $+65^\circ$ , avoiding crowded regions near the Galactic plane (Drake et al. 2009). The observations were obtained unfiltered in order to maximize the throughput, and then the magnitudes were transformed to an approximate  $V$  magnitude ( $V_{\text{CSS}}$ ; Drake et al. 2014a).

Drake et al. (2014b) investigated the properties of 367 ultrashort-period binary candidates identified from CSS data. Papageorgiou et al. (2018) reported an updated catalogue of 4683 eclipsing Algol-type binaries (EA) from the CSS survey. The physical parameters of the EA systems were explored by Lee (2015), Papageorgiou et al. (2019), and Carmo et al. (2020). Using the same sample of 4683 EA in CSS, Papageorgiou et al. (2021) reported 126 EAs with possible quadratic or cyclic period variations. We focus on the initial sample of Drake et al. (2014a) of 30 743 eclipsing binaries classified as EWs. This sample was explored by Marsh et al. (2017), who characterize 9380 EWs, and more recently by Sun et al. (2020), who presented the physical parameters of 2335 late-type EWs.

### 2.2 Identification of LMRs

Our first step was to exclude from the initial sample systems with insufficiently sampled LCs that have less than 150 observations ( $N_p$ ) and periods longer than  $\sim 0.8$  d, resulting in a sample of 30 592 systems (sample 1). To remove outliers and poor measurements, we first cleaned the LCs of this sample using  $3\sigma$  clipping along the phase-folded LCs, adopting the period from Drake et al. (2014a). Then the initial epoch values were determined using an iterative procedure of fitting a second-degree polynomial to the deeper eclipse. As a result of this procedure, we redetermined the ephemerides of the systems.

As the components of LMRs are characterized by a large difference between their masses, and hence their radii, it is expected that their LCs should exhibit flat bottoms of long duration, compared to common EWs. Since the main idea was to take advantage of the LC morphology, we compiled the LCs of 42 well-studied LMRs from the literature (sample 2) on the basis of their mass ratios, the totality of the eclipses, and the availability of their  $V$ -band LCs.

These are indicated in Table A1 with ‘\*’. For 26 systems from sample 2 that are also identified as extreme LMRs by Şenavcı et al. (2016), the LCs from the *Kepler* mission (Koch et al. 2010) were used. Although *Kepler*’s  $K_p$  filter is essentially a broad VR, its high-accuracy photometry provides valuable information for studies of the LC morphology.

We performed Fourier decomposition (FD) of the phase-folded, normalized flux LCs of both samples, based on the following equation (e.g. Deb & Singh 2009):

$$m(t) = A_0 + \sum_{j=1}^{10} \{a_j \sin[2\pi j\phi(t)] + b_j \cos[2\pi j\phi(t)]\}, \quad (1)$$

where  $m(t)$  is the observed magnitude at time  $t$ ,  $A_0$  is the mean magnitude,  $a_j$ ,  $b_j$  are the amplitude components of the  $(j-1)$ th harmonic, and  $\phi(t)$  is the phase (in the range [0–1]) corresponding to a full cycle, with the zero-point of the phased LC corresponding to the primary (deeper) minimum. As to the number of terms to be used in the FD, we choose a high order because otherwise the flat part of the total eclipse cannot be properly reproduced.

We analysed the full set of  $a_j$ ,  $b_j$  coefficients (20 in total), and arrived at the conclusion that the higher order coefficients, especially  $b_8$ , are more efficient in identifying LMRs than are the lower order ones. This can be appreciated from Fig. 1, which shows the distribution of the  $b_6$ ,  $b_8$ , and  $b_9$  coefficients, and where the literature and new candidate LMRs (blue solid circles and red solid squares, respectively) occupy a separate position from the other EWs (grey points). After this analysis, sample 1 was reduced to 2101 candidates. The LCs of the stars in this sample were then subjected to visual inspection, focusing on the totality and duration of the eclipses, finally leading to our sample of 30 new LMR candidates. Table 1 lists the coordinates (RA and Dec), reference time of minimum (in Heliocentric Julian Day,  $HJD_0$ ), period ( $P$ ), the CSS magnitude at maximum light ( $V_{\text{CSS}}(\text{max})$ ), the mean photometric error ( $\sigma_{\text{CSS}}$ ), and the number of available CSS observations ( $N_p$ ) of the 30 new CSS LMRs. The overestimated original CSS photometric errors were corrected by using the correction factor provided by Graham et al. (2017), based on the analytical expression derived by Papageorgiou et al. (2018, their footnote 8).

## 3 LIGHT-CURVE MODELLING

The photometric data of the 30 CSS LMR candidates were analysed using PHOEBE-scripter (Prša & Zwitter 2005) to determine the systems’ physical parameters. In the absence of spectroscopic data (as it is often the case for relatively dim,  $V > 13$  mag, EWs), the totality provides the most reliable photometric value for the mass ratio (Terrell & Wilson 2005; Hambálek & Pribulla 2013; Şenavcı et al. 2016). This is usually performed by initializing a 2D grid search on the mass ratio ( $q$ )–inclination ( $i$ ) plane, setting ‘overcontact not in thermal contact’ mode where  $q = M_2/M_1$  is the mass ratio of the system.<sup>1</sup> As we wanted to explore the systems parameter space of the solutions and investigate how well the area of global minimum is mapped in the case of LMRs given the photometry cadence and precision of CSS survey, a synthetic light curve (LC) of a LMR system ( $q = 0.096$ ,  $i = 81^\circ 4$ ) was generated using PHOEBE-scripter. The LC mimics the observational data of CSS having 350 data points and photometric errors around 0.01 mag. The synthetic LC (red

<sup>1</sup>Throughout this work we use number 1 (2) for the more (less) massive component, which is considered to be the primary (secondary).

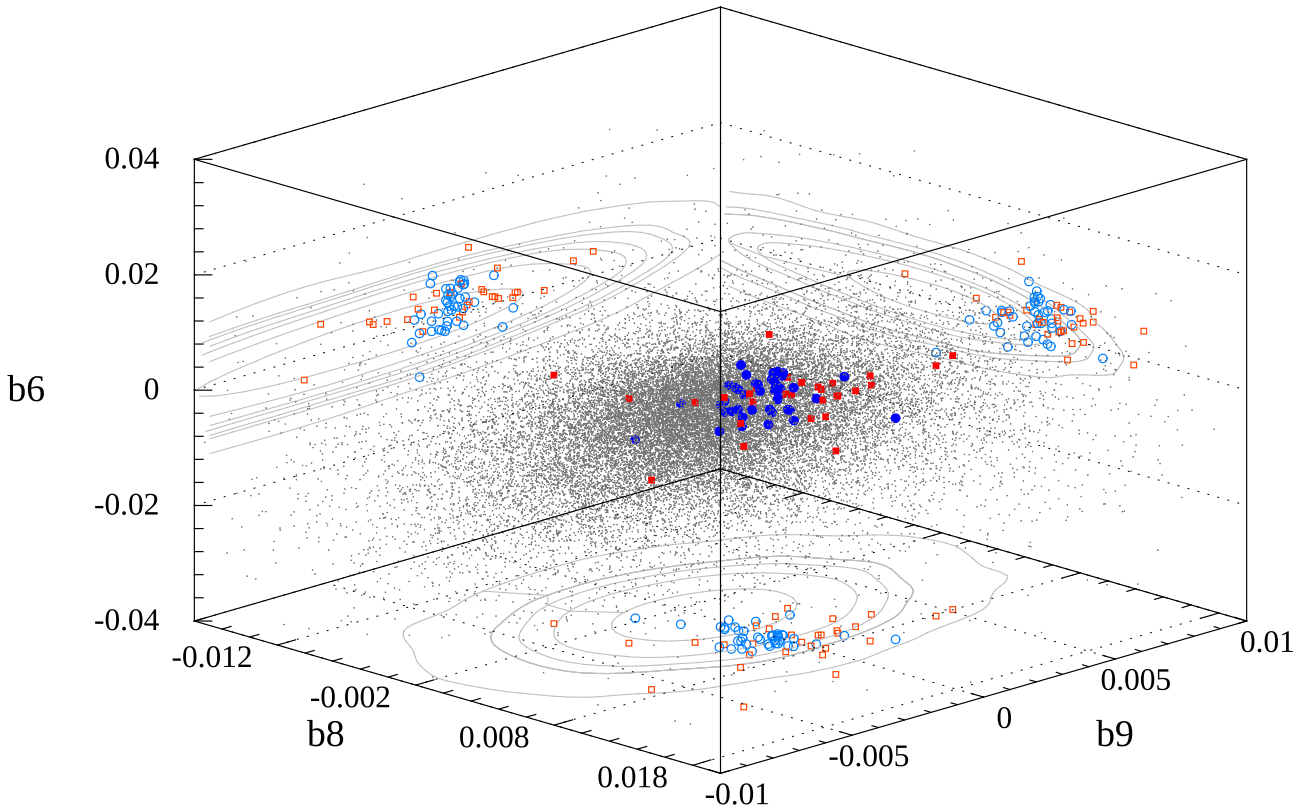


**Figure 1.** A 3D plot of  $b_6$ ,  $b_8$ , and  $b_9$  FD coefficients of sample 1 EWs represented by grey points and sample 2 (systems from literature, see text for description) represented by solid blue circles. The new CSS candidates (solid red squares) are located on the right top. Contour lines represent the projected distribution of EWs in each plane, while the light blue open circles and light red open squares are the projections of the literature and new LMR systems, respectively.

points) with the photometric errors and the solution (blue line) are shown in Fig. 2 (top panel), whereas the bottom panel of Fig. 2 represents the 2D distribution of  $\log \chi^2$  values in the  $(q, \sin i)$  plane. The solution  $(q_{\min}, i_{\min})$ , as it emerges from the  $q-i$  scan, is  $(0.1, 83^\circ)$ , which is in very good agreement with the real solution of the synthetic system, thus confirming the applicability of the method on this sample.

Following the results of the above test, for a rough estimation of the solution  $(q_{\min}, i_{\min})$ , which was obtained by  $\chi^2$  minimization, the range of explored  $q$  values was set to  $[0.1-0.6]$ , and that of  $i$  values to  $[68^\circ-90^\circ]$ , with step sizes of 0.05 and  $1^\circ$ , respectively. Then, depending on the results, the range was set to  $q_{\min} \pm 0.05$  with a step 0.01 for two runs, one without phase shift and another with phase shift 0.5. During this  $q-i$  scan, the effective temperature of the primary star  $T_1$ , the mass ratio  $q$ , and the orbital inclination  $i$  were set as fixed parameters, while the effective temperature  $T_2$  of the secondary, the modified potential  $\Omega = \Omega_{1,2}$ , and the passband luminosity of the primary  $L_1$  were set as adjustable parameters. Fig. 3 exhibits representative examples of the  $q-i$  scan for four new CSS LMRs.

### 3.1 Initial models for PHOEBE-scripter

To initialize the models, an estimation of the system's temperature is needed since the LC morphology can only constrain the ratio of the components' temperatures ( $T_2/T_1$ ). The effective temperature of the primary was fixed at the system's value ( $T_{\text{sys}}$ ) given by Stassun et al. (2019). This was derived from either spectroscopy or from empirical relations between  $T_{\text{eff}}$  and the  $G_{\text{BP}} - G_{\text{RP}}$  colour

(DR2; Gaia Collaboration et al. 2018), based on a set of 19 962 stars having spectroscopically determined  $T_{\text{eff}}$  and being within 100 pc so as to avoid reddening. Taking into account that  $T_{\text{sys}}$  is dominated by the temperature of the primary (hotter) component, we set  $T_{\text{sys}} = T_1$ . Limb-darkening coefficients were interpolated from van Hamme (1993) tables for the given temperatures, while gravity-darkening coefficients  $g$  and surface albedos  $A$  were accordingly assumed for convective ( $g = 0.32, A = 0.5$ ) or radiative envelopes ( $g = 1, A = 1$ ). The synchronization parameters were set as  $F = 1$ , assuming synchronous rotation of the components. Having set the above parameters and before the  $q-i$  scan is performed, the ephemeris of each system was refined by adjusting the reference time of minimum (HJD<sub>0</sub>) in PHOEBE. The resulting values of  $q$  and  $i$ , along with corresponding  $T_2$ ,  $\Omega_{1,2}$ , and  $L_1$  acquired from the fine scan of the parameter space, were used as input parameters to check the solution for each system. The final parameters  $q$ ,  $T_2/T_1$ ,  $\Omega_{1,2}$ ,  $r_1$ ,  $r_2$ ,  $i$ ,  $L_1/L_{\text{tot}}$ , and  $f^2$  are presented in Table 2, where  $r_1, r_2$  are the mean volume radii of the components and  $L_1/L_{\text{tot}}$  is the ratio of the bandpass luminosity of the primary component to the total bandpass luminosity. The LCs of the improved final models are shown in Fig. A1. Four systems (CSS\_J080724.7+164610, CSS\_J082850.5+015641, CSS\_J110526.4+285617, and CSS\_J155637.0+060949) show significant period variation of the order of  $10^{-6} \text{ d yr}^{-1}$  during the 9 yr of CSS data. The third light contribution was also investigated and found to be negligible ( $\leq 1$  per cent) in the context of our photometric

<sup>2</sup>  $f = \frac{\Omega_{\text{out}} - \Omega_{\text{in}}}{\Omega_{\text{out}} + \Omega_{\text{in}}}$ , where  $f$  is the fill-out factor, and  $\Omega_{\text{in}}$  and  $\Omega_{\text{out}}$  are the modified potential of the inner and the outer Lagrangian points, respectively.

**Table 1.** The 30 new LMR candidates selected from sample 1 using Fourier decomposition (FD).

ID	RA <sub>J2000</sub> ( $^{\text{h}}\text{:}\text{m}\text{:}\text{s}$ )	Dec. <sub>J2000</sub> ( $^{\circ}\text{:}\text{'}\text{.}\text{"}$ )	HJD <sub>0</sub> (245 0000+)	Period (d)	$V_{\text{CSS}}(\text{max})$ (mag)	$\sigma_{\text{CSS}}$ (mag)	$N_p$
CSS_J011848.4+132107	01:18:48.49	+13:21:07.6	6589.79386	0.3439788	13.21	0.01	300
CSS_J015301.5+223638	01:53:01.55	+22:36:38.4	3653.82712	0.2594140	15.92	0.03	274
CSS_J021552.4+324419	02:15:52.41	+32:44:19.5	5120.91902	0.5737980	14.68	0.02	350
CSS_J022044.4+280006	02:20:44.42	+28:00:06.1	4405.81533	0.7593753	14.42	0.02	356
CSS_J030702.2+261521	03:07:02.24	+26:15:21.8	5648.62161	0.7283894	13.98	0.02	374
CSS_J051156.6+011756	05:11:56.63	+01:17:56.5	3703.75981	0.7527221	14.82	0.02	351
CSS_J075839.9+131355	07:58:39.98	+13:13:55.7	6358.70319	0.4620180	14.88	0.02	293
CSS_J075848.2+125656	07:58:48.24	+12:56:56.1	4922.69449	0.3499800	14.08	0.02	293
CSS_J080724.7+164610	08:07:24.78	+16:46:10.6	5211.84350	0.3629629	14.39	0.02	415
CSS_J082140.8+192034	08:21:40.85	+19:20:34.5	5240.76455	0.4323400	15.15	0.02	528
CSS_J082850.5+015641	08:28:50.52	+01:56:41.1	5301.61530	0.4886486	13.37	0.01	346
CSS_J082916.5+131557	08:29:16.54	+13:15:57.6	5321.64675	0.3729305	13.98	0.02	438
CSS_J084222.2+041155	08:42:22.24	+04:11:55.5	4588.65898	0.2809483	15.67	0.03	381
CSS_J093010.1-021624	09:30:10.15	-02:16:24.9	5240.80316	0.3214746	15.56	0.03	318
CSS_J103653.7-072753	10:36:53.79	-07:27:53.6	5652.74006	0.2444613	15.75	0.03	276
CSS_J110526.4+285617	11:05:26.44	+28:56:17.2	4977.70007	0.3491059	14.93	0.02	388
CSS_J112643.3-141735	11:26:43.32	-14:17:35.7	4537.84328	0.3116524	13.60	0.01	156
CSS_J120945.8-025729	12:09:45.87	-02:57:29.2	5596.86649	0.3114363	15.29	0.02	294
CSS_J134010.1+134515	13:40:10.17	+13:45:15.2	5919.99314	0.4110526	14.29	0.02	380
CSS_J134512.0+034251	13:45:12.07	+03:42:51.1	3762.98614	0.4240236	15.22	0.02	349
CSS_J145437.2+060239	14:54:37.21	+06:02:39.8	4917.95998	0.5436659	15.28	0.02	351
CSS_J155637.0+060949	15:56:37.09	+06:09:49.3	4477.02450	0.3605211	15.81	0.03	357
CSS_J161753.6+205014	16:17:53.67	+20:50:14.1	4954.82770	0.5098331	14.60	0.02	379
CSS_J163819.6+034852	16:38:19.65	+03:48:52.0	6158.79806	0.2053320	14.26	0.02	339
CSS_J210300.1+050345	21:03:00.14	+05:03:45.6	4235.88388	0.5921606	13.90	0.01	387
CSS_J211420.2-142710	21:14:20.28	-14:27:10.8	5530.59888	0.5981238	15.32	0.02	297
CSS_J233821.8+200518	23:38:21.81	+20:05:18.2	6167.79999	0.3545902	13.23	0.01	324
CSS_J234145.7+233158	23:41:45.73	+23:31:58.6	4391.81504	0.5986466	13.91	0.01	309
CSS_J234324.8+211100	23:43:24.84	+21:11:00.4	5585.57623	0.6310680	14.50	0.02	332
CSS_J234807.2+193717	23:48:07.21	+19:37:17.8	5590.60823	0.3800130	15.46	0.03	331

accuracy in one filter. However in the past, several systems showing low-amplitude LCs on the *Hipparcos* mission (Selam 2004) were later spectroscopically found to be triples and the true mass ratio and/or inclination angle was higher.

### 3.2 Error estimation of the physical parameters

In our analysis we consider that the uncertainty of the mass ratio ( $\delta q$ ) is determined by the step of the grid search, thus we set  $\delta q = 0.010$ . In some cases, the global minimum of the  $\chi^2$  curve is broader and flatter, and so the uncertainty in  $q$  is underestimated. For these systems we consider the values of  $q$  around the global minimum that resulted to  $\chi^2$  increased up to 5 per cent of the minimum value ( $\chi^2_{\text{min}}$ ) and adopt the standard deviation of this area as  $\delta q$ . Thus, for 11 out of 30 systems  $\delta q = 0.010$ , while for the remainder it falls in the range  $0.010 < \delta q \leq 0.025$ . The temperature uncertainty of the systems is taken from Stassun et al. (2019). The uncertainties in the derived physical parameters are estimated by performing Monte Carlo simulations (Papageorgiou & Christopoulou 2015; Papageorgiou et al. 2019), since the formal errors from the fitting of the LC are heavily underestimated. During this procedure, each photometric point of the observed LC was randomly displaced 1000 times according to its photometric error  $\sigma_{\text{CSS}}$ , drawn from a normal distribution with zero mean and  $\sigma_{\text{CSS}}$  as standard deviation. The 1000 synthetic LCs, generated in this way, for each system were then fitted by only adjusting  $T_2$ ,  $\Omega_{1,2}$ ,  $L$ , and  $i$ . We finally extracted the lower and the upper error boundaries from each parameter distribution ( $q$ ,  $T_2/T_1$ ,

$\Omega_{1,2}$ ,  $r_1$ ,  $r_2$ ,  $i$ ,  $L_1/L_{\text{tot}}$ , and  $f$ ). The mean of these is the final error provided for each of these quantities in the final catalogue (Table 2).

Additionally one of the 30 candidates in our catalogue, namely CSS\_J011848.4+132107 (also known as EM Psc), has already been studied by Yang et al. (2005b), who found, using a V-band LC,  $(q_{\text{min}}, i_{\text{min}}) = (0.100, 83.3)$ . Qian et al. (2008), using  $R$ ,  $I$  band LCs, later found  $(0.1487, 88.6)$  for the same system. Our solution,  $(q_{\text{min}}, i_{\text{min}}) = (0.110 \pm 0.015, 89.6^{+0.8}_{-2.2})$  (see Table 2), is in accordance with Yang et al. (2005b), showing that  $V_{\text{CSS}}$  LCs can be used to estimate the systems' physical parameters.

### 3.3 Absolute parameters

In the absence of spectroscopic data, given the photometric mass ratio of EWs with total eclipses, the usual and simplest way to estimate the primary mass (and consequently  $M_2 = qM_1$ ) and semimajor axis ( $\alpha$ ) is using a spectral type–temperature and spectral type–mass calibration, under the assumption that the primary is on the main sequence (Cox 2000; Pecaut & Mamajek 2013). Other ways include an indirect path of statistically derived relations such as period–mass, period–semimajor axis, or equivalently the total mass of the system (Dimitrov & Kjurkchieva 2015; Yang & Qian 2015; Šenavc̄ et al. 2016). Another indirect method comes from the published 2D and 3D correlations involving combinations of  $M_1$ ,  $M_2$ ,  $R_1$ ,  $R_2$ ,  $L_1$ ,  $L_2$ ,  $P$ , and  $q$ , as given in Gazeas (2009) based on the data in Gazeas & Stępień (2008).

Alternatively, the absolute parameters of a binary can be estimated out of the absolute magnitude of the primary  $M_{V1}$ . This can be done

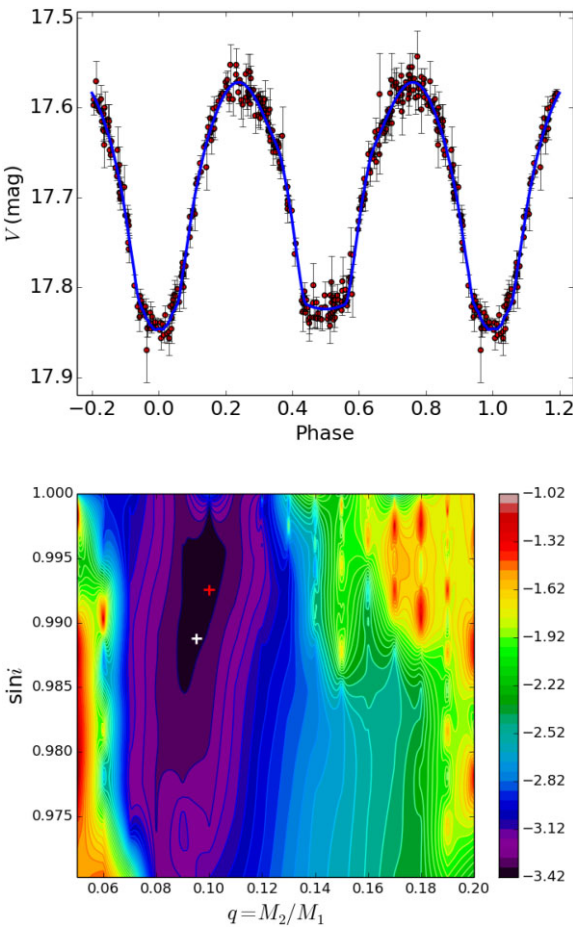


**Figure 2.** Top panel: synthetic LC with photometric errors generated using PHOEBE-scripter (red points). The blue line shows the solution given by our method. Bottom panel: contour plot of  $\log \chi^2$  (colour coded according to the scale on the right) in the  $(q, \sin i)$  plane of the synthetic system. The white cross represents the real solution of the synthetic system, while the red cross the resulting solution.

using the passband luminosity ratio of the photometric solution and the maximum magnitude of the system  $M_{\text{Vsys}}$ . The latter can be estimated directly from the data using the *Gaia* distance corrected for the interstellar extinction  $A_V$ . In the case of differential photometry,  $M_{\text{Vsys}}$  can be derived from a period–colour–magnitude relation, such as the one derived by Mateo & Rucinski (2017) based on *Gaia* Data Release 1 (DR1) data (318 EWs) or by Chen et al. (2019) based on *Gaia* DR2 measurements. Next,  $M_{\text{V1}}$  is converted to  $M_{\text{bol}}$  based on the bolometric correction (BC) corresponding to the temperature derived from the photometric solution. Finally, the primary mass  $M_1$  is estimated if a mass–luminosity ( $M$ – $L$ ) relation  $L \sim M^\alpha$  is used, under the assumption, well supported by the empirical data, that primary components of contact systems lie in general between the zero-age main sequence (ZAMS) and the terminal-age main sequence (TAMS; Yakut & Eggleton 2005). Sun et al. (2020) used  $\alpha = 4.216$  (Yıldız & Doğan 2013) to infer the mass of the primary. Lu et al. (2020) suggested a method that combined the PAdova and TRieste Stellar Evolution Code (PARSEC; Bressan et al. 2012) with the Roche geometric model to determine the masses of EWs. They applied their method on a sample of 140 spectroscopic studied binaries, and found it to be efficient in high-mass ratio and short-period systems with low effective temperatures.

In this study, we tested all the above methods and empirical relations, as we wanted to select those that provide a better description of the data. For this, we compiled a sample of 161 EWs from Yıldız & Doğan (2013) and Latković, Čeki & Lazarević (2021) with spectroscopically derived mass ratios, since spectroscopic studies are known to produce results with the highest accuracy. This provides us with an extensive and highly heterogeneous sample. We performed a linear fitting in the  $\log M$ – $\log L$  plane of the massive component of this spectroscopic sample. By randomly selecting the mass and luminosity errors from the available literature errors, this fitting was repeated  $10^5$  times. Then, the best pair  $(b, a)$  in the relation  $\log L = \log b + a \log M$  is represented by the mean value of the region where the above fittings have the lowest absolute percentage error (up to 10 per cent) between the calculated and spectroscopic masses. The corresponding uncertainties were derived from the standard deviation of the  $b$  and  $a$  values in the same region. Thus, we derived  $b = 0.63 \pm 0.04$  and  $a = 4.8 \pm 0.2$ . With these values, the above relation predicts the observed masses within  $\Delta M_1 \leq 10$  per cent for 65 per cent of the systems and within  $\Delta M_1 \leq 20$  per cent for 90 per cent of the systems, where  $\Delta M_1 = M_{1,\text{obs}} - M_{1,\text{rel}}$  is the average fractional mass difference,  $M_{1,\text{obs}}$  represents the mass from the analysis of spectroscopic data, and  $M_{1,\text{rel}}$  is the mass obtained from the relation. Nevertheless, we caution that there are several factors that, if not properly accounted for in the analysis, may affect the inferred luminosities of the components, and thereby their masses. This includes, among the others, spots due to magnetic activity, presence of circumstellar material, and third light contributions. In the case of a spotted system, for instance, the inferred luminosities (hence masses) may very well depend on the phase of the magnetic cycle during which the observations are carried out.

We decided to follow the second path and estimate the absolute magnitude of the primary. We cross-matched the LMR sample with *Gaia* Early Data Release 3 (EDR3; Bailer-Jones et al. 2021) using a matching radius of 2 arcsec to find the corresponding distances. The distances of 60 per cent of the sources are  $\leq 2$  kpc. For each source, we also calculate the total line-of-sight Galactic extinction from the 3D dust reddening map of Green et al. (2019), derived from *Gaia* parallaxes and stellar photometry from the Panoramic Survey Telescope and Rapid Response System 1 (Pan-STARRS 1) and the Two Micron All-Sky Survey (2MASS) data. The magnitude of the primary is estimated from the magnitude at quadratures of the system using the results of Table 2 ( $L_1/L_{\text{tot}}$ ). The magnitudes were transformed to Johnson  $V$  based on the relation of Drake et al. (2013). The temperatures of the individual components were derived from disentangling the value of the binary temperature (see Section 3.1) using equation (3) of Zwitter et al. (2003), the ratio of relative radii  $r_2/r_1$  and the temperature ratio  $T_2/T_1$  from the LC analysis (see Table 2). Then the absolute bolometric magnitude is derived based on the bolometric correction (from Bessell, Castelli & Plez 1998) corresponding to the effective temperature of the primary, and the primary luminosity is obtained. Finally, the mass of the primary components was estimated from our derived mass–luminosity relation, and consequently the mass of the secondaries from the mass ratio, the semimajor axis from Kepler’s law, and the mean radii from the corresponding relative radii.

To calculate the uncertainties of the component’s effective temperature ( $\sigma_{T_1}, \sigma_{T_2}$ ), we considered the uncertainty of the systems’ effective temperatures from the *Transiting Exoplanet Survey Satellite* (TESS) Input Catalog, v-8.0 (TIC-8) as the dominant source of error, since the temperature ratio  $T_2/T_1$  uncertainty contribution is of the order  $\sim 10$  K, while the ratio of relative radii  $r_2/r_1$  uncertainty contribution is negligible. The remaining uncertainties

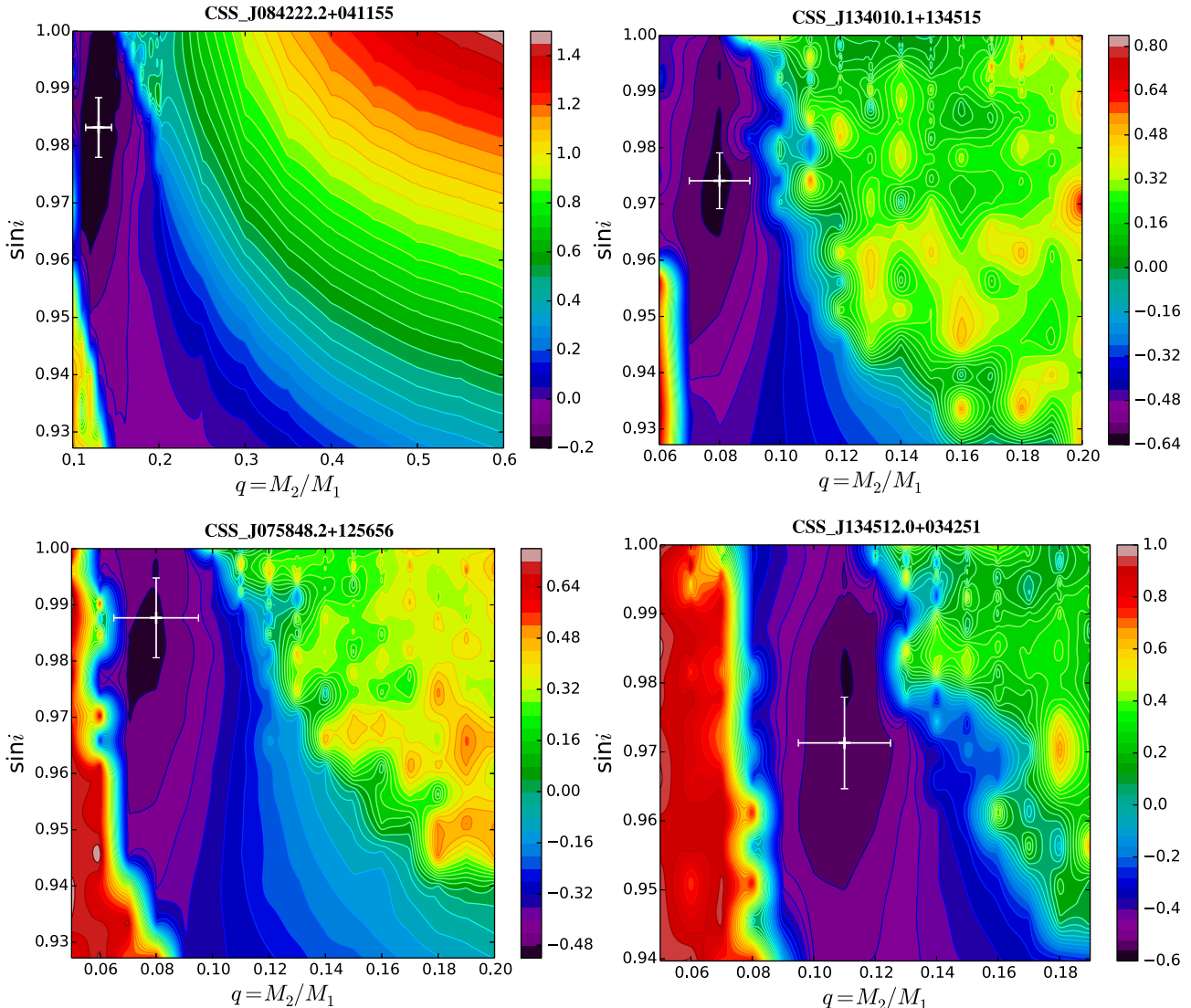


**Figure 3.** Contour plots of  $\log \chi^2$  (colour coded according to the scale on the right) in the  $(q, \sin i)$  plane of four CSS LMRs. The white crosses represent the solutions of the systems with the error bars derived from the Monte Carlo procedure.

were calculated considering the photometric error from the LCs, the uncertainty in the  $B - V$  colours (calculated from  $\sigma_B$ ,  $\sigma_V$ , as given by TIC-8), and the uncertainty of the distance estimation combined with the estimated errors of the physical parameters (Section 3.2). The results are given in Table 3.

#### 4 RESULTS AND DISCUSSION

It can be seen from Table 3 that the new LMRs have mean primary mass  $1.42 \pm 0.26 M_{\odot}$ , and mean secondary mass  $0.177 \pm 0.048 M_{\odot}$ . Half of the systems have temperatures in the range 5000–6500 K, while the hottest reaches 7280 K, and there is no preference between A or W subtypes. There are five systems with temperature difference between the components ( $\Delta T$ ) above 500 K, with the mean being about 260 K. We also find no trend in which  $\Delta T$  increases with increasing temperature or with decreasing fill-out factor.

The evolutionary status of these new CSS LMRs can be compared in the mass–radius plane with 173 LMRs compiled from the literature having  $q \leq 0.25$  derived spectroscopically or/and having total eclipse (listed in Table A1). The main source of Table A1 comes from

Latković et al. (2021), but we have excluded systems that have unreliable or peculiarly large or small masses, corrected or updated the absolute parameters of others, and also included new systems. We also did not include LMRs from the automated modelling of Sun et al. (2020) and Li, Liu & Zhang (2020), as we wanted to focus on dedicated studies of LMRs. Fig. 4 shows their location in the  $\log M$ – $\log R$  diagram together with ZAMS and TAMS loci calculated for solar metallicity using the Binary Star Evolution (BSE) code (Hurley, Tout & Pols 2002). The primary and secondary components are gathered in two different areas, above ZAMS and TAMS, respectively, indicating their different status but also their difference with the main-sequence stars of the same mass.

It can be seen from Table 2 that ~40 per cent of the 30 new LMRs are deep contact ( $f \geq 50$  per cent) with  $q \leq 0.25$ , and that eight of them, within the errors, belong to the class of extreme LMRs with  $q \leq 0.1$ . Thus, with our 17 new discoveries, there are 43 extreme LMRs, only six of which have spectroscopic mass ratios (listed in Table A1). The latter include the peculiar AW UMa, which shows the largest difference between photometric and spectroscopic mass ratio,  $q = 0.076$  (Eaton 2016) and  $q = 0.099$  (Rucinski 2015, 2020),

**Table 2.** The physical parameters of the 30 new CSS LMRs derived by LC modelling.

ID	$q$	$\frac{T_2}{T_1}$	$\Omega_{12}$	$r_1$	$r_2$	$i$ ( $^{\circ}$ )	$\frac{L_1}{L_{\text{tot}}}$	$f$
CSS_J011848.4+132107	$0.110 \pm 0.015$	$0.975 \pm 0.003$	$1.940 \pm 0.002$	$0.594 \pm 0.001$	$0.237 \pm 0.001$	$89.6 \pm 2.0$	0.883	$0.68 \pm 0.03$
CSS_J015301.5+223638	$0.200 \pm 0.015$	$1.026 \pm 0.006$	$2.186 \pm 0.008$	$0.539 \pm 0.003$	$0.269 \pm 0.003$	$80.0 \pm 1.0$	0.782	$0.36 \pm 0.06$
CSS_J021552.4+324419	$0.110 \pm 0.010$	$0.920 \pm 0.006$	$1.971 \pm 0.005$	$0.580 \pm 0.002$	$0.221 \pm 0.003$	$79.3 \pm 2.0$	0.909	$0.25 \pm 0.07$
CSS_J022044.4+280006	$0.150 \pm 0.010$	$0.944 \pm 0.005$	$2.063 \pm 0.007$	$0.563 \pm 0.003$	$0.249 \pm 0.003$	$84.7 \pm 1.0$	0.870	$0.41 \pm 0.07$
CSS_J030702.2+261521	$0.090 \pm 0.015$	$0.952 \pm 0.005$	$1.903 \pm 0.002$	$0.599 \pm 0.001$	$0.213 \pm 0.001$	$81.2 \pm 0.7$	0.910	$0.42 \pm 0.04$
CSS_J051156.6+011756	$0.150 \pm 0.010$	$0.925 \pm 0.006$	$2.072 \pm 0.009$	$0.560 \pm 0.004$	$0.245 \pm 0.004$	$83.1 \pm 2.4$	0.882	$0.32 \pm 0.10$
CSS_J075839.9+131355	$0.070 \pm 0.010$	$0.869 \pm 0.012$	$1.834 \pm 0.009$	$0.621 \pm 0.004$	$0.203 \pm 0.006$	$70.0 \pm 2.1$	0.947	$0.61 \pm 0.19$
CSS_J075848.2+125656	$0.080 \pm 0.015$	$0.974 \pm 0.006$	$1.870 \pm 0.003$	$0.609 \pm 0.002$	$0.207 \pm 0.002$	$81.0 \pm 2.6$	0.909	$0.48 \pm 0.07$
CSS_J080724.7+164610	$0.150 \pm 0.015$	$1.006 \pm 0.003$	$2.058 \pm 0.002$	$0.565 \pm 0.001$	$0.251 \pm 0.001$	$88.5 \pm 1.2$	0.836	$0.46 \pm 0.03$
CSS_J082140.8+192034	$0.100 \pm 0.010$	$0.966 \pm 0.006$	$1.921 \pm 0.002$	$0.597 \pm 0.001$	$0.226 \pm 0.001$	$75.1 \pm 1.0$	0.891	$0.59 \pm 0.03$
CSS_J082850.5+015641	$0.180 \pm 0.015$	$1.001 \pm 0.002$	$2.132 \pm 0.003$	$0.550 \pm 0.001$	$0.265 \pm 0.001$	$85.7 \pm 0.9$	0.816	$0.44 \pm 0.02$
CSS_J082916.5+131557	$0.190 \pm 0.010$	$1.037 \pm 0.002$	$2.158 \pm 0.003$	$0.545 \pm 0.001$	$0.267 \pm 0.001$	$83.3 \pm 1.1$	0.786	$0.41 \pm 0.02$
CSS_J084222.2+041155	$0.130 \pm 0.015$	$1.016 \pm 0.006$	$2.000 \pm 0.007$	$0.579 \pm 0.003$	$0.245 \pm 0.003$	$79.5 \pm 1.6$	0.845	$0.56 \pm 0.08$
CSS_J093010.1-021624	$0.110 \pm 0.020$	$1.031 \pm 0.006$	$1.921 \pm 0.003$	$0.603 \pm 0.001$	$0.249 \pm 0.002$	$78.0 \pm 2.3$	0.842	$0.96 \pm 0.03$
CSS_J103653.7-072753	$0.180 \pm 0.010$	$1.070 \pm 0.005$	$2.175 \pm 0.011$	$0.535 \pm 0.004$	$0.246 \pm 0.004$	$82.9 \pm 2.2$	0.768	$0.06 \pm 0.04$
CSS_J110526.4+285617	$0.110 \pm 0.015$	$1.031 \pm 0.005$	$1.923 \pm 0.003$	$0.602 \pm 0.001$	$0.248 \pm 0.002$	$85.8 \pm 2.4$	0.839	$0.93 \pm 0.04$
CSS_J112643.3-141735	$0.120 \pm 0.020$	$1.033 \pm 0.004$	$1.950 \pm 0.003$	$0.595 \pm 0.001$	$0.253 \pm 0.002$	$79.3 \pm 1.5$	0.834	$0.88 \pm 0.04$
CSS_J120945.8-025729	$0.140 \pm 0.015$	$1.073 \pm 0.005$	$1.989 \pm 0.003$	$0.588 \pm 0.001$	$0.270 \pm 0.002$	$81.2 \pm 2.1$	0.787	$0.95 \pm 0.03$
CSS_J134010.1+134515	$0.080 \pm 0.010$	$0.964 \pm 0.006$	$1.876 \pm 0.003$	$0.607 \pm 0.001$	$0.204 \pm 0.001$	$76.9 \pm 1.3$	0.913	$0.37 \pm 0.05$
CSS_J134512.0+034251	$0.110 \pm 0.015$	$0.966 \pm 0.007$	$1.970 \pm 0.006$	$0.581 \pm 0.003$	$0.221 \pm 0.003$	$79.2 \pm 1.6$	0.889	$0.27 \pm 0.08$
CSS_J145437.2+060239	$0.110 \pm 0.010$	$0.914 \pm 0.009$	$1.959 \pm 0.008$	$0.586 \pm 0.003$	$0.227 \pm 0.004$	$79.3 \pm 1.6$	0.909	$0.43 \pm 0.11$
CSS_J155637.0+060949	$0.120 \pm 0.025$	$1.033 \pm 0.007$	$1.944 \pm 0.009$	$0.598 \pm 0.002$	$0.257 \pm 0.003$	$75.9 \pm 1.6$	0.833	$0.96 \pm 0.04$
CSS_J161753.6+205014	$0.080 \pm 0.010$	$0.980 \pm 0.008$	$1.894 \pm 0.003$	$0.598 \pm 0.001$	$0.193 \pm 0.002$	$78.0 \pm 1.3$	0.912	$0.04 \pm 0.02$
CSS_J163819.6+034852	$0.150 \pm 0.015$	$0.999 \pm 0.004$	$2.034 \pm 0.003$	$0.575 \pm 0.001$	$0.263 \pm 0.002$	$87.1 \pm 1.8$	0.833	$0.71 \pm 0.03$
CSS_J210300.1+050345	$0.100 \pm 0.015$	$0.912 \pm 0.005$	$1.937 \pm 0.003$	$0.590 \pm 0.001$	$0.217 \pm 0.001$	$82.8 \pm 1.2$	0.917	$0.34 \pm 0.04$
CSS_J211420.2-142710	$0.110 \pm 0.020$	$1.126 \pm 0.006$	$1.976 \pm 0.010$	$0.578 \pm 0.004$	$0.218 \pm 0.004$	$74.3 \pm 1.2$	0.814	$0.18 \pm 0.10$
CSS_J233821.8+200518	$0.220 \pm 0.015$	$1.003 \pm 0.002$	$2.236 \pm 0.009$	$0.531 \pm 0.003$	$0.275 \pm 0.003$	$86.3 \pm 2.6$	0.790	$0.33 \pm 0.06$
CSS_J234145.7+233158	$0.090 \pm 0.015$	$1.000 \pm 0.006$	$1.882 \pm 0.002$	$0.610 \pm 0.001$	$0.226 \pm 0.001$	$77.7 \pm 0.9$	0.884	$0.78 \pm 0.04$
CSS_J234324.8+211100	$0.110 \pm 0.010$	$0.994 \pm 0.005$	$1.941 \pm 0.002$	$0.594 \pm 0.001$	$0.237 \pm 0.001$	$80.6 \pm 1.0$	0.870	$0.68 \pm 0.03$
CSS_J234807.2+193717	$0.180 \pm 0.020$	$1.044 \pm 0.005$	$2.137 \pm 0.006$	$0.551 \pm 0.002$	$0.265 \pm 0.003$	$87.9 \pm 1.8$	0.786	$0.40 \pm 0.05$

**Table 3.** The absolute parameters of the 30 new CSS LMRs.

ID	$T_{\text{sys}}$ (K)	$T_1$ (K)	$T_2$ (K)	$M_1$ ( $M_{\odot}$ )	$M_2$ ( $M_{\odot}$ )	$R_1$ ( $R_{\odot}$ )	$R_2$ ( $R_{\odot}$ )	$L_1$ ( $L_{\odot}$ )	$L_2$ ( $L_{\odot}$ )	$\frac{f_s}{f_o}$	$\left(\frac{J_s}{J_o}\right)_k$
CSS_J011848.4+132107	$5723 \pm 100$	$5742 \pm 101$	$5600 \pm 99$	$1.25 \pm 0.05$	$0.14 \pm 0.02$	$1.37 \pm 0.02$	$0.55 \pm 0.01$	$1.85 \pm 0.34$	$0.26 \pm 0.02$	0.217	0.195
CSS_J015301.5+223638	$4811 \pm 175$	$4786 \pm 174$	$4909 \pm 180$	$0.97 \pm 0.02$	$0.19 \pm 0.02$	$0.97 \pm 0.01$	$0.48 \pm 0.01$	$0.55 \pm 0.06$	$0.12 \pm 0.02$	0.110	0.171
CSS_J021552.4+324419	$6801 \pm 176$	$6863 \pm 178$	$6315 \pm 169$	$1.70 \pm 0.07$	$0.19 \pm 0.02$	$2.08 \pm 0.03$	$0.79 \pm 0.01$	$8.03 \pm 1.29$	$0.89 \pm 0.10$	0.207	0.117
CSS_J022044.4+280006	$6702 \pm 229$	$6760 \pm 231$	$6382 \pm 220$	$1.89 \pm 0.09$	$0.28 \pm 0.02$	$2.56 \pm 0.04$	$1.13 \pm 0.02$	$13.64 \pm 2.37$	$1.90 \pm 0.27$	0.150	0.092
CSS_J030702.2+261521	$6646 \pm 63$	$6680 \pm 63$	$6362 \pm 70$	$1.84 \pm 0.07$	$0.17 \pm 0.03$	$2.57 \pm 0.03$	$0.91 \pm 0.01$	$11.72 \pm 1.62$	$1.23 \pm 0.06$	0.264	0.148
CSS_J051156.6+011756	$6344 \pm 156$	$6414 \pm 158$	$5936 \pm 152$	$1.73 \pm 0.08$	$0.26 \pm 0.02$	$2.45 \pm 0.04$	$1.07 \pm 0.02$	$8.76 \pm 1.58$	$1.28 \pm 0.14$	0.148	0.089
CSS_J075839.9+131355	$6643 \pm 138$	$6714 \pm 140$	$5833 \pm 145$	$1.51 \pm 0.06$	$0.11 \pm 0.02$	$1.83 \pm 0.03$	$0.60 \pm 0.02$	$4.57 \pm 0.70$	$0.37 \pm 0.04$	0.356	0.187
CSS_J075848.2+125656	$6095 \pm 25$	$6111 \pm 25$	$5951 \pm 41$	$1.32 \pm 0.04$	$0.11 \pm 0.02$	$1.43 \pm 0.01$	$0.49 \pm 0.01$	$2.39 \pm 0.24$	$0.27 \pm 0.01$	0.303	0.229
CSS_J080724.7+164610	$5991 \pm 22$	$5984 \pm 22$	$6022 \pm 31$	$1.25 \pm 0.03$	$0.19 \pm 0.02$	$1.37 \pm 0.01$	$0.61 \pm 0.01$	$1.86 \pm 0.20$	$0.44 \pm 0.01$	0.151	0.140
CSS_J082140.8+192034	$7097 \pm 158$	$7126 \pm 159$	$6882 \pm 159$	$1.56 \pm 0.07$	$0.16 \pm 0.02$	$1.72 \pm 0.02$	$0.65 \pm 0.01$	$5.38 \pm 0.94$	$0.86 \pm 0.08$	0.239	0.131
CSS_J082850.5+015641	$6428 \pm 35$	$6426 \pm 35$	$6433 \pm 38$	$1.47 \pm 0.05$	$0.26 \pm 0.02$	$1.73 \pm 0.02$	$0.83 \pm 0.01$	$4.04 \pm 0.45$	$1.06 \pm 0.03$	0.124	0.076
CSS_J082916.5+131557	$6051 \pm 24$	$6006 \pm 24$	$6226 \pm 28$	$1.27 \pm 0.04$	$0.24 \pm 0.01$	$1.36 \pm 0.01$	$0.67 \pm 0.01$	$1.98 \pm 0.26$	$0.60 \pm 0.02$	0.117	0.109
CSS_J084222.2+041155	$6325 \pm 168$	$6310 \pm 168$	$6408 \pm 174$	$1.19 \pm 0.05$	$0.16 \pm 0.02$	$1.15 \pm 0.02$	$0.49 \pm 0.01$	$1.49 \pm 0.27$	$0.36 \pm 0.04$	0.179	0.181
CSS_J093010.1-021624	$5746 \pm 224$	$5720 \pm 223$	$5894 \pm 232$	$1.17 \pm 0.04$	$0.13 \pm 0.02$	$1.30 \pm 0.02$	$0.54 \pm 0.01$	$1.35 \pm 0.22$	$0.31 \pm 0.05$	0.224	0.236
CSS_J103653.7-072753	$5446 \pm 227$	$5487 \pm 229$	$5287 \pm 222$	$1.05 \pm 0.04$	$0.19 \pm 0.01$	$0.94 \pm 0.01$	$0.43 \pm 0.01$	$0.74 \pm 0.14$	$0.13 \pm 0.02$	0.117	0.159
CSS_J110526.4+285617	$5297 \pm 210$	$5273 \pm 209$	$5435 \pm 216$	$1.17 \pm 0.06$	$0.13 \pm 0.02$	$1.37 \pm 0.02$	$0.57 \pm 0.01$	$1.37 \pm 0.32$	$0.25 \pm 0.04$	0.224	0.234
CSS_J112643.3-141735	$5557 \pm 148$	$5528 \pm 147$	$5709 \pm 153$	$1.14 \pm 0.03$	$0.14 \pm 0.02$	$1.25 \pm 0.01$	$0.53 \pm 0.01$	$1.17 \pm 0.11$	$0.27 \pm 0.03$	0.203	0.229
CSS_J120945.8-025729	$5640 \pm 159$	$5563 \pm 157$	$5967 \pm 171$	$1.12 \pm 0.05$	$0.16 \pm 0.01$	$1.23 \pm 0.02$	$0.57 \pm 0.01$	$1.09 \pm 0.21$	$0.36 \pm 0.04$	0.174	0.206
CSS_J134010.1+134515	$6924 \pm 35$	$6949 \pm 36$	$6695 \pm 53$	$1.52 \pm 0.06$	$0.12 \pm 0.02$	$1.66 \pm 0.02$	$0.56 \pm 0.01$	$4.71 \pm 0.70$	$0.56 \pm 0.02$	0.301	0.159
CSS_J134512.0+034251	$7006 \pm 188$	$7035 \pm 189$	$6797 \pm 190$	$1.62 \pm 0.07$	$0.18 \pm 0.03$	$1.68 \pm 0.02$	$0.64 \pm 0.01$	$6.47 \pm 1.06$	$0.78 \pm 0.09$	0.208	0.116
CSS_J145437.2+060239	$6861 \pm 192$	$6930 \pm 194$	$6336 \pm 189$	$1.68 \pm 0.10$	$0.18 \pm 0.02$	$2.02 \pm 0.04</$					

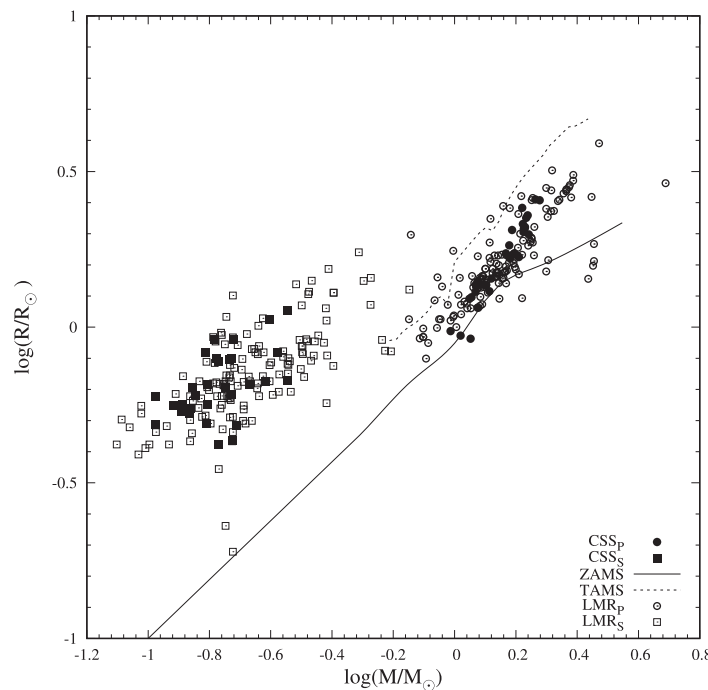


**Figure 4.** The primary and secondary components of CSS LMRs (solid circles and solid squares, respectively), combined with primary and secondary components from previous LMRs from the literature (open circles and open squares, respectively), plotted on the  $\log M$ - $\log R$  diagram. Zero-age main sequence (ZAMS; solid) and terminal-age main sequence (TAMS; dotted) lines at solar metallicity, as obtained using the BSE code (Hurley et al. 2002), are overplotted.

respectively. The remaining five systems are SX CrV, V870 Ara, KR Com, FP Boo, and XX Sex. The system with the highest fill-out factor ( $f \sim 99$  per cent) is KR Com, which also has a large third light contribution at the level of 60 per cent, while SX CrV is the system with the lowest fill-out factor ( $f \sim 27$  per cent). As can be seen in Fig. 5, where all previously known LMRs are plotted together with EWs with spectroscopic mass ratio ( $EW_{sp}$ ) and new CSS LMRs, the smallest the  $q$  value, the larger the fill-out factor distribution range. It is obvious that in previous LMRs that have both total eclipses and spectroscopic mass ratio, the symbols coincide.

#### 4.1 Pre-merger candidates

According to Hut (1980), a binary system becomes unstable if the ratio of the sum of the spin angular momenta of the stars ( $J_s$ ) to the orbital angular momentum ( $J_o$ ) exceeds  $\sim 1/3$  (Darwin's instability), and is heading towards merging because the companion star can no longer keep the primary star synchronously rotating via the tidal interaction.

To investigate the stability of the 30 new LMRs listed in Tables 1–3, we determine this ratio using the formula derived from equations (1) and (2) of Li & Zhang (2006):

$$\frac{J_s}{J_o} = \frac{(1+q)}{q} (k_1 r_1)^2 \left[ 1 + q \left( \frac{k_2}{k_1} \right)^2 \left( \frac{r_2}{r_1} \right)^2 \right], \quad (2)$$

where  $q$  is the mass ratio of the system and  $k_1, k_2$  are the dimensionless gyration radii of both components. The estimation of the gyration radii is crucial for the above estimation even when the mass ratio of the system is known spectroscopically, since it depends on the internal structure of the star. Main-sequence stars tend to have gyration radii from 0.075 (fully radiative) to 0.205 (fully convective). Assuming  $k_1^2 = k_2^2 = k^2 = 0.06$  (Sun like) as in Rasio (1995) and Li & Zhang (2006), the results for the 30 new LMRs are plotted in Fig. 6.

It is seen in Fig. 6 and in Tables 3 and A1 that the majority of the systems lies in the region limited between the inner and outer Roche lobes. Nevertheless, CSS J075839.9+131355, V1187 Her, V857 Her, ASAS 083241+2332, V53 (in the globular cluster M4=NGC 6121), and six contact binaries from Kepler Input Catalog (KIC; KIC 4244929, KIC 9151972, KIC 11097678, KIC 8539720, KIC 3127873, and KIC 12352712) are in the instability area, i.e. have surpassed the  $J_s/J_o = 1/3$  limit, and accordingly should have already merged. Alternative solutions that take into account phase smearing, as proposed by Zola et al. (2017), may be possible for the KICs. Three of them with periods  $P > 0.67$  d may have different  $q, i$  model when third light is included in the *Kepler* LC with binned data. V53 is a member of the globular cluster M4, and a blue straggler with a decreasing period (Kaluzny, Thompson & Krzeminski 1997; Li et al. 2017). We therefore reestimate the ratio  $\frac{J_s}{J_o}$  assuming  $k_1^2 \neq k_2^2$  using the tabulated results of Landin, Mendes & Vaz (2009), which take into account the combined effects of tidal and rotational distortions on a star in a binary system. For different masses of the primary components in the ZAMS, we calculate  $k_1^2$  from the linear relationships, we derived as  $k_1 = -0.250 M + 0.539$  for stars with  $M = 0.5\text{--}1.4 M_\odot$  and  $k_1 = 0.014 M + 0.152$  for stars with  $M > 1.4 M_\odot$ , although in this range it can be considered approximately constant with a value of  $k_1 \approx 0.18$ . Jiang et al. (2010) also found that  $k^2$  decreases with increasing mass and age of the star if the star's mass is less than about  $1.3 M_\odot$ , and that above this mass  $k^2$  is roughly constant. For the secondary we assume  $k_2^2 \sim 0.205$ , in accordance with a fully convective star (Arbutina 2007), which is a good assumption as it is a very low mass star ( $M_2 < 0.3 M_\odot$ ), although we know that it is oversized compared to a main-sequence star of the same mass due to energy transfer. The results of the angular momentum ratio against the mass ratio  $q$  assuming different values of gyration radius for the two components are presented in Fig. 7.

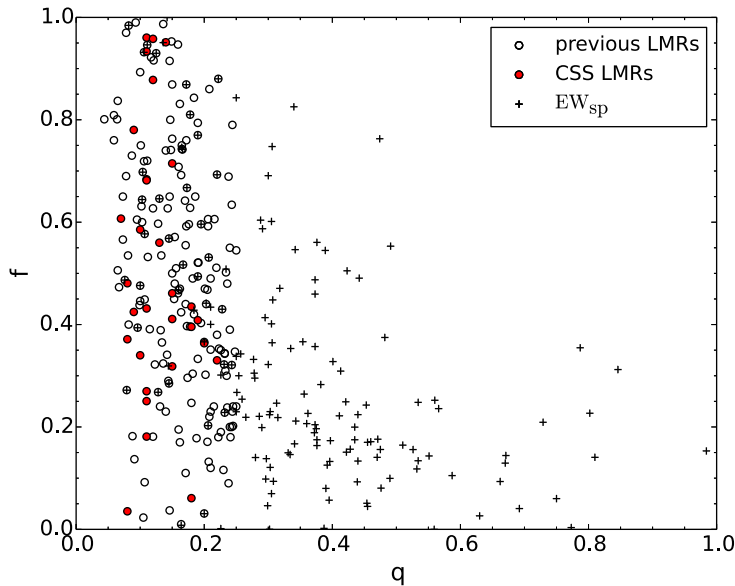


**Figure 5.** The relation  $q-f$  for all previous LMRs (open circles) from Table A1, new CSS LMRs (solid red circles), and EWs with spectroscopically derived mass ratios ( $EW_{sp}$ , crosses). In previous LMRs having both total eclipses and spectroscopic mass ratio, the symbols coincide.

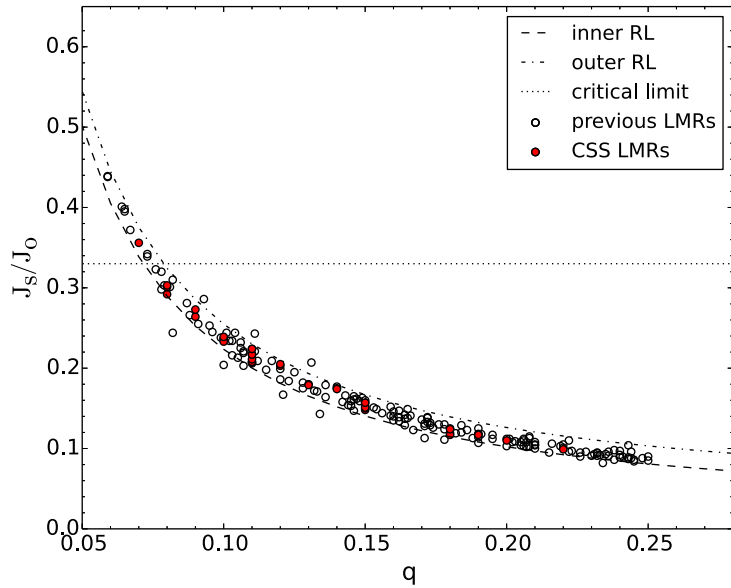


**Figure 6.** The angular momentum ratio  $J_s/J_0$  against the mass ratio  $q$  assuming  $k^2 = 0.06$  for both components of all previous LMRs (open circles) from Table A1 and new CSS LMRs (solid red circles). The dashed and dashed-dotted lines correspond to theoretical systems filling the inner and outer Roche lobes, respectively, and the dotted line to the instability limit  $J_s/J_0 = 0.33$ .

As seen from Fig. 7 and Tables 3 and A1, the scatter is larger than Fig. 6 but the majority of the LMRs has not surpassed the dynamical stability limit, with the exceptions of KR Com (0.489), ASAS J102556+2049.3 (0.456), ASAS J083241+2332.4 (0.354), and V1222 Tau (0.349), that should have already merged. Although these systems have different fill-out factors (99 per cent, 24 per cent, 51–70 per cent, and 53 per cent, respectively) and primary masses, all of them show indications of the presence of a third body. ASAS J102556+2049.3 has a large period decrease over 11 yr ( $dP/dt = -3.4 \times 10^{-6} \text{ d yr}^{-1}$ ; Kjurkchieva, Popov & Petrov 2019b), ASAS J083241+2332.4 shows a sinusoidal period variation (Sriram et al. 2016), the spectroscopically studied KR Com has a

third light contribution at the level of 60 per cent (Gazeas et al. 2021a), and V1222 Tau has one of the largest period variations  $dP/dt = +8.19 \times 10^{-6} \text{ d yr}^{-1}$  and an extreme O’Connell effect. Like in many LMRs, the long term period variations are associated with the presence of an additional component (Pribulla & Rucinski 2006) that plays a particular role in angular momentum evolution (Eggleton & Kisselova-Eggleton 2006). Some information on the possible triplicity could be obtained from the so-called astrometric overnoise parameter renormalized unit weight error (RUWE) in the *Gaia* EDR3 (Stassun & Torres 2021). This is an indicator for the multiplicity of a source when  $\geq 1.4$ , although according to Stassun & Torres (2021) RUWE values even slightly greater than 1.0

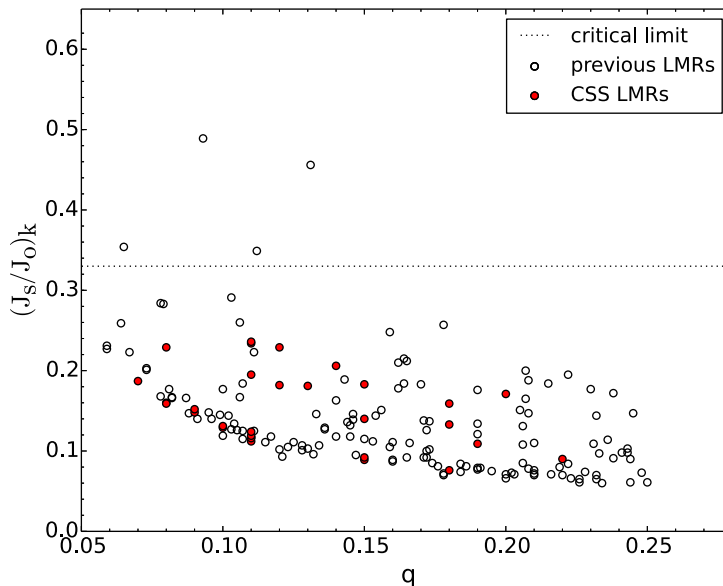


**Figure 7.** The angular momentum ratio  $\left(\frac{J_s}{J_o}\right)_k$  against the mass ratio  $q$  assuming different values of  $k_1^2$  for the massive component and  $k_2^2 \sim 0.205$  for the less massive component. The symbols are as in Fig. 6.

may signify unresolved binaries in *Gaia* EDR3. Only two systems, CSS\_J011848.4+132107 (EM Psc) and CSS\_J233821.8+200518 have RUWE 3.6 and 3.7, respectively, whereas 17 CSS LMRs have slightly greater than 1.0 as it is the case of CSS\_J110526.4+285617 (1.112) and CSS\_J155637.0+060949 (1.024) that have also large orbital period variation. However, *Gaia* is insensitive to short-period triples and systems where photocentre does not move significantly (see fig. 4 in Belokurov et al. 2020). This is the case of systems detected by *TESS* with  $\text{RUWE} < 1.4$  like TIC 388459317 (0.952), TIC 52041148 (1.052) (Borkovits et al. 2022), or even quadruples like TIC 278956474 (1.06; Rowden et al. 2020) where the low RUWE value suggests the two binaries are likely to be tightly bound.

Nevertheless, the uncertainty in the determination of the mass of the primary component, and consequently  $k_1$ , determines the uncertainty of the  $\frac{J_s}{J_o}$  ratio. Under the assumption that the primary is a typical main-sequence star with an effective temperature of e.g. 5880–5440 K, corresponding to spectral types G0–G8, a mass uncertainty of 16 per cent results to an uncertainty of  $\pm 24$  per cent of the  $\frac{J_s}{J_o}$  ratio. Thus, we consider additionally as potential pre-mergers, systems with  $(J_s/J_o)_k \sim 0.3$ , like ZZ PsA, SX CrV, and ASAS J165139+2255.7. For ZZ PsA, our result is consistent with the recent study of Wadhwa et al. (2021b), who characterized ZZ PsA as a bright nova progenitor by developing a new relationship among the mass of the primary, the instability mass ratio  $q_{\text{inst}}$ , and the degree of contact. Following their methodology, we estimated for V1222 Tau, SX CrV, and ASAS J165139+2255.7 the ratio of the reported photometric mass ratio to the instability mass ratio  $q/q_{\text{inst}}$  to be 0.89, 1.08, and 0.96, respectively, at a separation and period  $(1.95 R_\odot, 0.3143 \text{ d})$  for V1222 Tau,  $(0.204 R_\odot, 0.292 \text{ d})$  for SX CrV, and  $(2.24 R_\odot, 0.363251 \text{ d})$  for ASAS J165139+2255.7, suggesting that these systems will enter an unstable phase. ASAS J083241+2332.4 and KR Com have  $q/q_{\text{inst}} = (0.85, 0.65)$ , as well as theoretical instability separation and period  $(2.29 R_\odot, 0.3515 \text{ d})$  and  $(2.763 R_\odot, 0.543028 \text{ d})$ , respectively. Among the new CSS LMRs, CSS\_J075848.2+125656, with  $q/q_{\text{inst}} = 1.23 \pm 0.23$ , and CSS\_J093010.1–021624, with  $q/q_{\text{inst}} = 1.25 \pm 0.23$ , can be considered as merging system candidates.

## 5 CONCLUSIONS

In this paper, we mine and model 30 new totally eclipsing CSS LMRs. We present their physical parameters ( $T_2/T_1$ ,  $R_2/R_1$ ,  $\Omega_{1,2}$ ,  $i$ ,  $f$ ) and the systems' global parameters, as determined from the LC solutions and *Gaia* EDR3 distances.

Normally, LMRs should have a deep contact configuration, but the existence also of systems far away from this expected state may indicate different evolutionary states. LMRs presenting a shallow or medium degree of contact may be the result of mass transfer from the less massive to the more massive component, which causes the orbit to enlarge without breaking the contact. In the case of a high contact degree, the surface of the binary is very close to its outer critical Roche lobe, and a long-term period decrease due to mass transfer or angular momentum loss via magnetic braking can cause the orbit to tighten, the inner and outer critical Roche lobes to shrink, and the degree of contact to increase. In the case of a high contact degree with continuous mass transfer from the more massive to the less massive (increasing period), and mass loss from the second Lagrange point ( $L_2$ ), the orbit of the system is contracting, with the mass ratio decreasing, and the evolution ends with a rapidly rotating single star. Tidal friction in the presence of a circumstellar disc or a third (or more) companion(s) can constitute another possible mechanism of angular momentum or mass loss (Tutukov, Dremova & Svechnikov 2004; Martin, Spruit & Tata 2011).

Why do systems with a lower mass ratio than theoretically predicted for stability exist? If the observations do not support the Darwin instability criterion in such systems, maybe the mechanism of merger is a different one, or we need to reconsider the parameters involved. Primarily since the primary's dimensionless gyration radius  $k_1$  depends on the primary's mass  $M_1$ , in the case of a photometric solution with total eclipse,  $M_1$  estimation is based on various assumptions that need to be reexamined. In addition, more realistic calculations should include the decrease of  $k_1$  with evolution (Jiang et al. 2010), or the decrease of  $\frac{k_2}{k_1}$  due to the differential rotation of the components (Hilditch 2001). The latter has been proposed as a mechanism for the energy transfer between the components (Yakut & Eggleton 2005; Eggleton 2010b).

Looking at the prototype of mergers, V1309 Sco, that was dominated in its final stage by  $L_2$  mass loss, another possible explanation is that the non-conservative mass and angular momentum loss drives the Darwin criterion and the instability mass ratio to lower values, as proposed by Pejcha et al. (2017). Nevertheless, since the progenitor of V1309 Sco is proposed to be an eclipsing contact binary with period of about 1.4 d (Tyenda et al. 2011), maybe larger period systems need to be observed in contact phase. These are few and represent the very end of contact binaries with periods 1.3–1.5 d in the period distribution as initially noticed by Rucinski (1998) and is still confirmed in the plethora of new discoveries of surveys (Li et al. 2019; Jayasinghe et al. 2020). However, in the model proposed by Stępień (2011) the primary of the pre-burst contact binary V1309 Sco is a giant that recently filled its Roche lobe and whose contact phase is very short. Thus, the proposed progenitors of mergers may differ from EWs in both evolutionary state and duration of the contact phase. Considering the rapid period decay of V1309 Sco preceding the merging, we suggest to search for systems with large orbital period change rates ( $dP/dt$ ) in photometric surveys, in combination with detailed study of their evolutionary state through high-accuracy spectroscopic observations (Rucinski 2020), reconsidering the energy transfer models between the components and including systematic monitoring of times of minima of the already proposed merger candidates.

## ACKNOWLEDGEMENTS

AP gratefully acknowledges the support provided by the grant cofinanced by Greece and the European Union (European Social Fund – ESF) through the Operational Programme ‘Human Resources Development, Education and Lifelong Learning’ in the context of the project ‘Reinforcement of Postdoctoral Researchers – 2nd Cycle’ (MIS-5033021), implemented by the State Scholarships Foundation (IKY). CEFL acknowledges a post-doctoral fellowship from the CNPq, MCTIC/FINEP (CT-INFRA grant 0112052700), and the Embrace Space Weather Program for the computing facilities at INPE. This work made use of data products from the CSS survey. Support for MC is provided by ANID’s Millennium Science Initiative through grant ICN12\_12009, awarded to the Millennium Institute of Astrophysics (MAS), and by ANID’s Basal project FB210003. The CSS survey is funded by the National Aeronautics and Space Administration under Grant No. NNG05GF22G issued through the Science Mission Directorate Near-Earth Objects Observations Program. The CRTS survey is supported by the US National Science Foundation under grants AST-0909182, AST-1313422, AST-1413600, and AST-1518308.

We would like to thank the referee for constructive comments and recommendations that have improved the paper.

## DATA AVAILABILITY

The data underlying this paper are available in the paper and in its online supplementary material.

## REFERENCES

- Acerbi F., Barani C., Martignoni M., 2014, *New Astron.*, 31, 1
- Aliçavuş F., Soydugan F., 2017, in *AIP Conf. Proc. Vol. 1815, Turkish Physical Society 32nd International Physics Congress (TPS32)*. Am. Inst. Phys., New York, p. 080004
- Alton K. B., 2016, *J. Am. Assoc. Var. Star Obser.*, 44, 87
- Alton K. B., 2018, *J. Am. Assoc. Var. Star Obser.*, 46, 3
- Alvarez G. E., Sowell J. R., Williamon R. M., Lapasset E., 2015, *PASP*, 127, 742
- Arbutina B., 2007, *MNRAS*, 377, 1635
- Bailer-Jones C. A. L., Rybizki J., Fouesneau M., Demleitner M., Andrae R., 2021, *AJ*, 161, 147
- Barani C., Martignoni M., Acerbi F., 2017, *New Astron.*, 50, 73
- Barone F., di Fiore L., Milano L., Russo G., 1993, *ApJ*, 407, 237
- Belokurov V. et al., 2020, *MNRAS*, 496, 1922
- Bessell M. S., Castelli F., Plez B., 1998, *A&A*, 333, 231
- Borkovits T. et al., 2022, *MNRAS*, 510, 1352
- Bressan A., Marigo P., Girardi L., Salasnich B., Dal Cero C., Rubele S., Nanni A., 2012, *MNRAS*, 427, 127
- Broens E., 2013, *MNRAS*, 430, 3070
- Broens E., 2021, *MNRAS*, 501, 4935
- Bulut A., Bulut İ., Demircan O., 2016, *New Astron.*, 44, 35
- Capezzali D., Fiorucci M., Spogli C., 2008, *Inf. Bull. Var. Stars*, 5824, 1
- Carmo A., Ferreira Lopes C. E., Papageorgiou A., Jablonski F. J., Rodrigues C. V., Drake A. J., Cross N. J. G., Catelan M., 2020, *MNRAS*, 498, 2833
- Caton D., Gentry D. R., Samec R. G., Chamberlain H., Robb R., Faulkner D. R., Hill R., 2019, *PASP*, 131, 054203
- Chen X., Wang S., de Grijs R., Deng L., 2019, in de Bruijn J. H. J., ed., 53rd ESLAB Symposium: The Gaia Universe. ESA, Noordwijk, p. 60
- Christopoulou P. E., Parageorgiou A., Chrysopoulos I., 2011, *AJ*, 142, 99
- Cox A. N., 2000, *Allen’s Astrophysical Quantities*, 4th edn. AIP Press, New York
- Csák B., Kiss L. L., Vinkó J., Alfaro E. J., 2000, *A&A*, 356, 603
- Darwin G. H., 1879, *Proc. R. Soc. Lond.*, 29, 168
- Deb S., Singh H. P., 2009, *A&A*, 507, 1729
- Deb S., Singh H. P., 2011, *MNRAS*, 412, 1787
- Devarapalli S. P., Jagirdar R., Prasad R. M., Thomas V. S., Ahmed S. A., Gralapally R., Das J. P., 2020, *MNRAS*, 493, 1565
- Dimitrov D. P., Kjurkchieva D. P., 2015, *MNRAS*, 448, 2890
- Djurašević G. et al., 2013, *AJ*, 145, 80
- Drake A. J. et al., 2009, *ApJ*, 696, 870
- Drake A. J. et al., 2013, *ApJ*, 763, 32
- Drake A. J. et al., 2014a, *ApJS*, 213, 9
- Drake A. J. et al., 2014b, *ApJ*, 790, 157
- Eaton J. A., 2016, *MNRAS*, 457, 836
- Eggleton P. P., 2010a, *New Astron. Rev.*, 54, 45
- Eggleton P. P., 2010b, in Prša A., Zejdá M., eds, ASP Conf. Ser. Vol. 435, Binaries - Key to Comprehension of the Universe. Astron. Soc. Pac., San Francisco, p. 151
- Eggleton P. P., Kisselava-Eggleton L., 2006, *Ap&SS*, 304, 75
- El-Sadek M. A., Djurašević G., Essam A., Hanna M. A., Amin M. Y., Hayman Z. M., Awadalla N. S., 2019, *New Astron.*, 69, 21
- Erkan N., Ulaş B., 2016, *New Astron.*, 46, 73
- Gaia Collaboration et al., 2018, *A&A*, 616, A10
- Gazeas K. D., 2009, *Commun. Asteroseismol.*, 159, 129
- Gazeas K., Stępień K., 2008, *MNRAS*, 390, 1577
- Gazeas K. D. et al., 2005, *Acta Astron.*, 55, 123
- Gazeas K. D., Niarchos P. G., Zola S., Kreiner J. M., Rucinski S. M., 2006, *Acta Astron.*, 56, 127
- Gazeas K. et al., 2021a, *MNRAS*, 501, 2897
- Gazeas K. D. et al., 2021b, *MNRAS*, 502, 2879
- Gezer İ., Bozkurt Z., 2016, *New Astron.*, 44, 40
- Godfrey S. N., Leung K. C., Schmidt E. G., 1996, *Ap&SS*, 246, 291
- Gorda S. Y., Lyaptsev A. P., Sobolev A. M., 2015, *Astrophys. Bull.*, 70, 109
- Graham M. J., Djorgovski S. G., Drake A. J., Stern D., Mahabal A. A., Glikman E., Larson S., Christensen E., 2017, *MNRAS*, 470, 4112
- Green G. M., Schlafly E., Zucker C., Speagle J. S., Finkbeiner D., 2019, *ApJ*, 887, 93
- Guo D.-F., Li K., Hu S.-M., Jiang Y.-G., Gao D.-Y., Chen X., 2015, *Res. Astron. Astrophys.*, 15, 889
- Guo D.-F., Li K., Gao X., Gao D.-Y., Xu Z.-J., Sun G.-Y., Liu F., Zhang C.-M., 2020, *MNRAS*, 497, 3381
- Gürol B., Terzioglu Z., Gürsoytrak S. H., Gökyay G., Derman E., 2011, *Astron. Nachr.*, 332, 690
- Gürol B., Gürsoytrak S. H., Bradstreet D. H., 2015, *New Astron.*, 39, 9

- Hambálek Ľ., Pribulla T., 2013, *Contr. Astron. Obser. Skalnate Pleso*, 43, 27
- He J.-J., Qian S.-B., Soonthornthum B., Aungwerojwit A., Liu N.-P., Sarotsakulchai T., 2019, *Res. Astron. Astrophys.*, 19, 056
- Hilditch R. W., 2001, *An Introduction to Close Binary Stars*. Cambridge Univ. Press, Cambridge
- Hurley J. R., Tout C. A., Pols O. R., 2002, *MNRAS*, 329, 897
- Hut P., 1980, *A&A*, 92, 167
- Ivezić Ž. et al., 2019, *ApJ*, 873, 111
- Jayasinghe T. et al., 2020, *MNRAS*, 493, 4045
- Jiang D., Han Z., Wang J., Jiang T., Li L., 2010, *MNRAS*, 405, 2485
- Kaluzny J., Thompson I. B., Krzeminski W., 1997, *AJ*, 113, 2219
- Kandulapati S., Devarapalli S. P., Pasagada V. R., 2015, *MNRAS*, 446, 510
- Kim C.-H., Song M.-H., Park J.-H., Jeong M.-J., Kim H.-Y., Han C., 2019, *J. Astron. Space Sci.*, 36, 265
- Kjurkchieva D. P., Popov V. A., Petrov N. I., 2019a, *New Astron.*, 68, 20
- Kjurkchieva D. P., Popov V. A., Petrov N. I., 2019b, *AJ*, 158, 186
- Kjurkchieva D., Popov V., Eneva Y., Petrov N., 2020a, *Bulgarian Astron. J.*, 32, 71
- Kjurkchieva D. P., Popov V. A., Petrov N. I., 2020b, *New Astron.*, 77, 101352
- Koch D. G. et al., 2010, *ApJ*, 713, L79
- Kopacki G., Pigulski A., 1995, *Acta Astron.*, 45, 753
- Kovacs G., Hartman J. D., Bakos G. Á., 2019, *A&A*, 631, A126
- Kriwattanawong W., Poojon P., 2013, *Res. Astron. Astrophys.*, 13, 1330
- Landin N. R., Mendes L. T. S., Vaz L. P. R., 2009, *A&A*, 494, 209
- Latković O., Čeki A., 2021, *PASJ*, 73, 132
- Latković O., Čeki A., Lazarević S., 2021, *ApJS*, 254, 10
- Lee C.-H., 2015, *MNRAS*, 454, 2946
- Li K., Qian S. B., 2013a, *New Astron.*, 21, 46
- Li K., Qian S. B., 2013b, *New Astron.*, 22, 57
- Li K., Qian S. B., 2013c, *New Astron.*, 25, 12
- Li L., Zhang F., 2006, *MNRAS*, 369, 2001
- Li K., Hu S., Chen X., Guo D., 2017, *PASJ*, 69, 79
- Li K., Xia Q. Q., Hu S. M., Guo D. F., Chen X., 2018, *PASP*, 130, 074201
- Li K., Xia Q.-Q., Michel R., Hu S.-M., Guo D.-F., Gao X., Chen X., Gao D.-Y., 2019, *MNRAS*, 485, 4588
- Li X.-Z., Liu L., Zhang X.-D., 2020, *PASJ*, 72, 66
- Liao W. P., Qian S. B., Soonthornthum B., Sarotsakulchai T., Zhu L. Y., Zhang J., Irina V., 2017, *PASP*, 129, 124204
- Liu L., Qian S. B., Fernández-Lajús E., 2011, *MNRAS*, 415, 1509
- Liu L., Qian S. B., Fernández Lajús E., 2014a, *New Astron.*, 26, 116
- Liu L. et al., 2014b, *New Astron.*, 31, 60
- Liu L., Qian S.-B., Soonthornthum B., Zhu L., He J.-J., Zhao E.-G., 2015, *PASJ*, 67, 74
- Liu L., Qian S., Zhu L., Liao W., He J., Liu N., 2017, *New Astron.*, 51, 1
- Lu L.-N., Liu J.-Z., Jiang D.-K., Wang Y.-H., 2020, *Res. Astron. Astrophys.*, 20, 196
- Luo X., Wang K., Zhang X., Deng L., Luo Y., Luo C., 2017, *AJ*, 154, 99
- Marsh F. M., Prince T. A., Mahabal A. A., Bellm E. C., Drake A. J., Djorgovski S. G., 2017, *MNRAS*, 465, 4678
- Martin E. L., Spruit H. C., Tata R., 2011, *A&A*, 535, A50
- Mateo N. M., Rucinski S. M., 2017, *AJ*, 154, 125
- Molnar L. A. et al., 2017, *ApJ*, 840, 1
- Na W. W., Qian S. B., Zhang L., Liao W. P., Soonthornthum B., Zhu L. Y., Zhao E. G., Zhou X., 2014, *New Astron.*, 30, 105
- Nakano S. et al., 2008, *IAU Circ.*, 8972, 1
- Oh K.-D., Kim C.-H., Kim H.-I., Lee W.-B., 2007, in Kang Y. W., Lee H.-W., Leung K.-C., Cheng K.-S., eds, *ASP Conf. Ser. Vol. 362, The Seventh Pacific Rim Conference on Stellar Astrophysics*. Astron. Soc. Pac., San Francisco, p. 82
- Oh K.-D., Kim H.-I., Sung E.-C., 2010, *J. Astron. Space Sci.*, 27, 69
- Ostadnezhad S., Delband M., Hasanzadeh A., 2014, *New Astron.*, 31, 14
- Özkardeş B., Erdem A., Bakış V., 2009, *New Astron.*, 14, 461
- Papageorgiou A., Christopoulou P. E., 2015, *AJ*, 149, 168
- Papageorgiou A., Catelan M., Christopoulou P.-E., Drake A. J., Djorgovski S. G., 2018, *ApJS*, 238, 4
- Papageorgiou A., Catelan M., Christopoulou P.-E., Drake A. J., Djorgovski S. G., 2019, *ApJS*, 242, 6
- Papageorgiou A., Catelan M., Christopoulou P.-E., Drake A. J., Djorgovski S. G., 2021, *MNRAS*, 503, 2979
- Pecaut M. J., Mamajek E. E., 2013, *ApJS*, 208, 9
- Pejcha O., Metzger B. D., Tyles J. G., Tomida K., 2017, *ApJ*, 850, 59
- Peng Y.-J. et al., 2016, *Res. Astron. Astrophys.*, 16, 157
- Poro A., Zamanpour S., Hashemi M., Aladağ Y., Aksaker N., Rezaei S., Solmaz A., 2021, *New Astron.*, 86, 101571
- Prasad V., Pandey J. C., Patel M. K., Srivastava D. C., 2013, *New Astron.*, 20, 52
- Pribulla T., Rucinski S. M., 2006, *AJ*, 131, 2986
- Pribulla T., Chochol D., Vanko M., Parimucha S., 2002, *Inf. Bull. Var. Stars*, 5258, 1
- Pribulla T., Vanko M., Hambalek L., 2009, *Inf. Bull. Var. Stars*, 5886, 1
- Prša A., Zwitter T., 2005, *ApJ*, 628, 426
- Qian S. B., Yang Y. G., Soonthornthum B., Zhu L. Y., He J. J., Yuan J. Z., 2005a, *AJ*, 130, 224
- Qian S. B., Zhu L. Y., Soonthornthum B., Yuan J. Z., Yang Y. G., He J. J., 2005b, *AJ*, 130, 1206
- Qian S. B., He J. J., Soonthornthum B., Liu L., Zhu L. Y., Li L. J., Liao W. P., Dai Z. B., 2008, *AJ*, 136, 1940
- Qian S. B., Liu L., Zhu L. Y., He J. J., Yang Y. G., Bernasconi L., 2011, *AJ*, 141, 151
- Qian S.-B., Zhu L.-Y., Liu L., Zhang X.-D., Shi X.-D., He J.-J., Zhang J., 2020, *Res. Astron. Astrophys.*, 20, 163
- Raghavan D. et al., 2010, *ApJS*, 190, 1
- Rappaport S., Deck K., Levine A., Borkovits T., Carter J., El Mellah I., Sanchis-Ojeda R., Kalomeni B., 2013, *ApJ*, 768, 33
- Rasio F. A., 1995, *ApJ*, 444, L41
- Robertson J. A., Eggleton P. P., 1977, *MNRAS*, 179, 359
- Rowden P. et al., 2020, *AJ*, 160, 76
- Rucinski S. M., 1998, *AJ*, 115, 1135
- Rucinski S. M., 2015, *AJ*, 149, 49
- Rucinski S. M., 2020, *AJ*, 160, 104
- Rucinski S. M., Pribulla T., van Kerkwijk M. H., 2007, *AJ*, 134, 2353
- Samec R., Corbin S., 2002, *Observatory*, 122, 22
- Samec R. G., Benkendorf B., Dignan J. B., Robb R., Kring J., Faulkner D. R., 2015, *AJ*, 149, 146
- Samec R. G., Gray C. R., Caton D., Faulkner D. R., Hill R., Hamme W. V., 2017, *J. Am. Assoc. Var. Star Obser.*, 45, 140
- Samec R. G., Caton D. B., Faulkner D. R., 2020, *J. Am. Assoc. Var. Star Obser.*, 48, 62
- Sarotsakulchai T. et al., 2018, *AJ*, 156, 199
- Saygan S., 2016, *New Astron.*, 46, 94
- Selam S. O., 2004, *A&A*, 416, 1097
- Selam S. O., Esmer E. M., Şenavcı H. V., Bahar E., Yörükoglu O., Yılmaz M., Baştürk Ö., 2018, *Ap&SS*, 363, 34
- Şenavcı H. V., Nelson R. H., Özavcı İ., Selam S. O., Albayrak B., 2008, *New Astron.*, 13, 468
- Şenavcı H. V., Doğruel M. B., Nelson R. H., Yılmaz M., Selam S. O., 2016, *Publ. Astron. Soc. Aust.*, 33, e043
- Socia Q. J., Welsh W. F., Short D. R., Orosz J. A., Angione R. J., Windmiller G., Caldwell D. A., Batalha N. M., 2018, *ApJ*, 864, L32
- Sriram K., Malu S., Choi C. S., Vivekananda Rao P., 2016, *AJ*, 151, 69
- Sriram K., Malu S., Choi C. S., Vivekananda Rao P., 2017, *AJ*, 153, 231
- Sriram K., Malu S., Choi C. S., Vivekananda Rao P., 2018, *AJ*, 155, 172
- Stassun K. G., Torres G., 2021, *ApJ*, 907, L33
- Stassun K. G. et al., 2019, *AJ*, 158, 138
- Stępień K., 2006, *Acta Astron.*, 56, 199
- Stępień K., 2009, *MNRAS*, 397, 857
- Stępień K., 2011, *A&A*, 531, A18
- Stępień K., Gazeas K., 2012, *Acta Astron.*, 62, 153
- Stępień K., Kiraga M., 2015, *A&A*, 577, A117
- Sun W., Chen X., Deng L., de Grijs R., 2020, *ApJS*, 247, 50
- Szalai T., Kiss L. L., Mészáros S., Vinkó J., Csizmadia S., 2007, *A&A*, 465, 943
- Terrell D., Wilson R. E., 2005, *Ap&SS*, 296, 221
- Tian X.-m., Zhu L.-y., Wang Z.-h., 2019, *PASP*, 131, 084203
- Tokovinin A., Thomas S., Sterzik M., Udry S., 2006, *A&A*, 450, 681

- Tutukov A. V., Dremova G. N., Svechnikov M. A., 2004, *Astron. Rep.*, 48, 219
- Tuvikene T., Eenmäe T., Sterken C., Brogt E., 2008, *Balt. Astron.*, 17, 79
- Tylenda R. et al., 2011, *A&A*, 528, A114
- Udalski A., 2003, *Acta Astron.*, 53, 291
- Ulaş B., Ulusoy C., 2014, *New Astron.*, 31, 56
- van Hamme W., 1993, *AJ*, 106, 2096
- Vaňko M., Parimucha Š., Pribulla T., Chochol D., 2004, *Balt. Astron.*, 13, 151
- Vinko J., Hegedus T., Hendry P. D., 1996, *MNRAS*, 280, 489
- Wadhwa S. S., 2004, *J. Am. Assoc. Var. Star Obser.*, 32, 95
- Wadhwa S. S., 2005, *Ap&SS*, 300, 329
- Wadhwa S. S., 2006, *Ap&SS*, 301, 195
- Wadhwa S. S., 2019, *J. Am. Assoc. Var. Star Obser.*, 47, 40
- Wadhwa S. S., Zealey W. J., 2004, *Ap&SS*, 291, 21
- Wadhwa S. S., Tothill N. F. H., DeHorta A. Y., Filipovic M., 2021a, *Res. Astron. Astrophys.*, 21, 235
- Wadhwa S. S., De Horta A. Y., Filipović M. D., Tothill N. F. H., Arbutina B., Petrović J., Djurašević G., 2021b, *MNRAS*, 501, 229
- Wang J.-J. et al., 2012, *PASJ*, 64, 83
- Wetterer C. J. et al., 2004, *Inf. Bull. Var. Stars*, 5547, 1
- Yakut K., Eggleton P. P., 2005, *ApJ*, 629, 1055
- Yakut K., Kalomeni B., İbanoğlu C., 2004, *A&A*, 417, 725
- Yang Y.-G., 2012, *Res. Astron. Astrophys.*, 12, 419
- Yang Y.-G., Qian S.-B., 2015, *AJ*, 150, 69
- Yang Y.-G., Qian S.-B., Zhu L.-Y., He J.-J., Yuan J.-Z., 2005a, *PASJ*, 57, 983
- Yang Y. G., Qian S. B., Gonzalez-Rojas D. J., Yuan J. Z., 2005b, *Ap&SS*, 300, 337
- Yang Y. G., Qian S. B., Zhang L. Y., Dai H. F., Soonthornthum B., 2013, *AJ*, 146, 35
- Yıldız M., Doğan T., 2013, *MNRAS*, 430, 2029
- Zhou X., Soonthornthum B., 2019, *PASJ*, 71, 39
- Zhou X., Qian S. B., Zhang J., Zhang B., Kreiner J., 2016a, *AJ*, 151, 67
- Zhou X., Qian S. B., Zhang J., Jiang L. Q., Zhang B., Kreiner J., 2016b, *ApJ*, 817, 133
- Zhou X., Qian S.-B., Zhang J., Li L.-J., Wang Q.-S., 2016c, *Adv. Astron.*, 2016, 746897
- Zhu L. Y., Qian S. B., Soonthornthum B., Yang Y. G., 2005, *AJ*, 129, 2806
- Zola S. et al., 2004, *Acta Astron.*, 54, 299
- Zola S., Gazeas K., Kreiner J. M., Ogloza W., Siwak M., Koziel-Wierzbowska D., Winiarski M., 2010, *MNRAS*, 408, 464
- Zola S., Baran A., Debski B., Jableka D., 2017, *MNRAS*, 466, 2488
- Zwitter T., Munari U., Marrese P. M., Prša A., Milone E. F., Boschi F., Tomov T., Siviero A., 2003, *A&A*, 404, 333

## APPENDIX A: PREVIOUS LMRS AND 30 NEW CSS LMRS

In this appendix, we provide 1) the observed LCs and the best fitted models of the 30 new CSS LMR systems (Figure A1) and 2) a compilation of LMRs, along with their parameters, from the literature and derived in this work (Table A1). The columns are organized as follows (from left to right): name, where (n) represents LMRs not included in Latković et al. (2021) and \* represents LMRs with LCs used for sample 2; period (in d); mass ratio ( $q$ ); method used to determine the mass ratio: photometric with total eclipses (T) or spectroscopic (SP); primary mass ( $M_1$ ); primary radius ( $R_1$ ); secondary radius ( $R_2$ ); fill-out factor ( $f$ ); the derived ratio of total spin angular to orbital momentum  $\frac{J_s}{J_o}$  for gyration radii  $k^2 = 0.06$  (this work); the derived ratio of total spin angular to orbital momentum  $\left(\frac{J_s}{J_o}\right)_k$  for different values of  $k_1^2$  for the massive component and  $k_2^2 \sim 0.205$  for the less massive component (this work); and references.

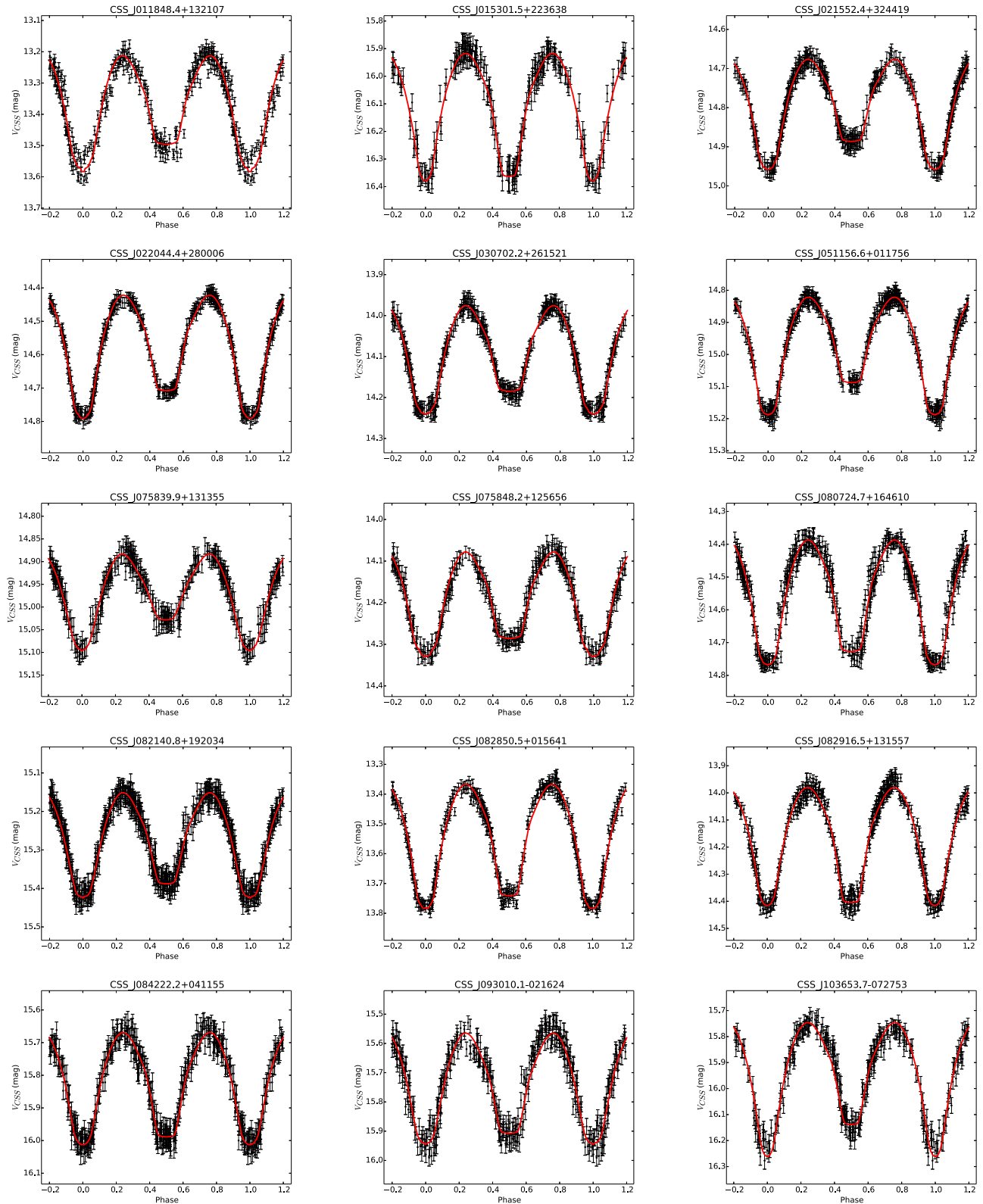


**Figure A1.** The observed LCs (black points) and the best-fitting models (red line) for the 30 new CSS LMR systems.

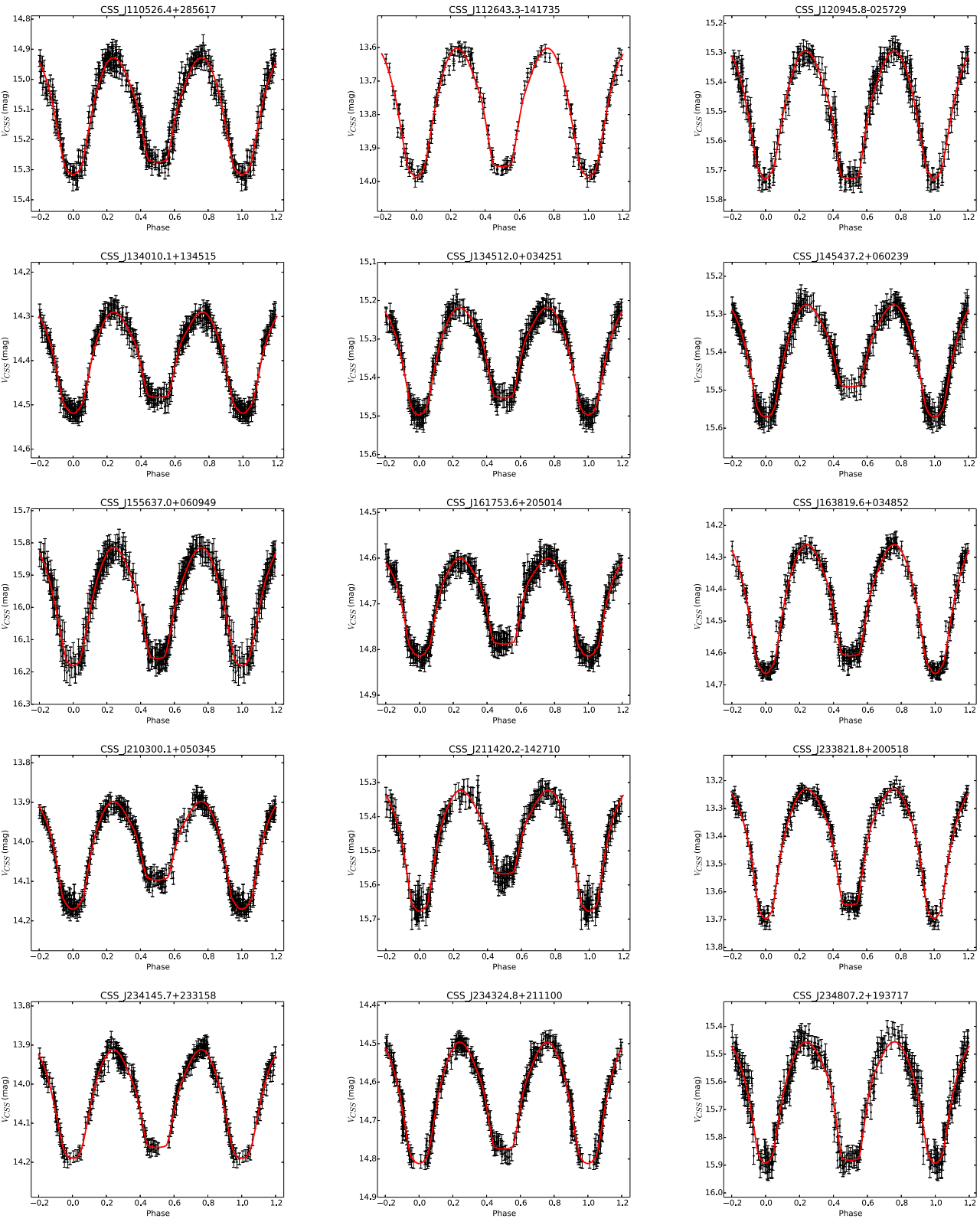


Figure A1. continued.

**Table A1.** Parameters of previously known LMRs.

Name	Period (d)	$q$	Type	$M_1$ ( $M_\odot$ )	$R_1$ ( $R_\odot$ )	$R_2$ ( $R_\odot$ )	$f$	$\frac{J_s}{J_0}$	$\left(\frac{J_s}{J_0}\right)_k$	Reference
V1187 Her	0.31076	0.044	T				0.801	0.612		Caton et al. (2019)
KIC 4244929*	0.34140	0.059	T	1.481	1.521	0.477	0.809	0.439	0.227	Şenavci et al. (2016)
KIC 9151972*	0.38680	0.059	T	1.606	1.696	0.528	0.760	0.438	0.231	Şenavci et al. (2016)
KIC 11097678*	0.99972	0.064 (0.097)	T	2.960	3.897	1.264	0.801 (0.87)	0.401	0.259	Şenavci et al. (2016); Zola et al. (2017)
ASAS J083241+2332.4*	0.31132	0.065	T	1.220	1.34	0.42	0.506	0.398	0.354	Sriram et al. (2016)
V857 Her*	0.38223	0.065	T				0.837	0.395		Qian et al. (2005b)
KIC 8539720*	0.74450	0.067 (0.158)	T	2.438	2.955	0.929	0.473 (0.860)	0.372	0.223	Şenavci et al. (2016); Zola et al. (2017)
KIC 3127873*	0.67153	0.073 (0.109)	T	2.268	2.69	0.899	0.65 (0.88)	0.342	0.201	Şenavci et al. (2016); Zola et al. (2017)
KIC 12352712*	0.72207	0.073	T	2.377	2.859	0.944	0.566	0.339	0.203	Şenavci et al. (2016)
AW UMa	0.43872	0.076 (0.099)	SP				0.487	0.323		Eaton (2016); Ruciński (2015)
ZZ PsA	0.37388	0.078	T	1.213	1.422	0.559	0.970	0.298	0.284	Wadhwa et al. (2021b)
M4 V53	0.30845	0.078	T	1.472	1.383	0.481	0.690	0.320	0.168	Li et al. (2017)
SX Crv	0.31660	0.079	SP	1.246	1.347	0.409	0.272	0.303	0.283	Zola et al. (2004)
KIC 10007533*	0.64806	0.081 (0.101)	T	2.199	2.566	0.881	0.535 (0.178)	0.301	0.177	Şenavci et al. (2016); Zola et al. (2017)
V870 Ara*	0.39972	0.082	SP	1.503	1.61	0.61	0.984	0.310	0.166	Szalai et al. (2007)
KIC 8145477*	0.56578	0.082 (0.102)	T	2.012	2.26	0.767	0.40 (0.650)	0.244	0.167	Şenavci et al. (2016); Zola et al. (2017)
KIC 11144556*	0.64298	0.087 (0.161)	T	2.174	2.542	0.927	0.730 (0.97)	0.281	0.166	Şenavci et al. (2016); Zola et al. (2017)
KIC 10596883*	0.46891	0.088	T	1.772	1.882	0.641	0.182	0.266	0.147	Şenavci et al. (2016)
KIC 8804824*	0.45740	0.091 (0.111)	T	1.738	1.829	0.628	0.137 (0.67)	0.255	0.140	Şenavci et al. (2016); Zola et al. (2017)
KR Com (n)	0.40797	0.093	SP	0.880	1.445	0.505	0.990	0.286	0.489	Gazeas et al. (2021a)
KIC 7698650*	0.59916	0.095 (0.123)	T	2.064	2.357	0.876	0.605 (0.700)	0.253	0.148	Şenavci et al. (2016); Zola et al. (2017)
FP Boo	0.64048	0.096	SP	1.614	2.31	0.774	0.394	0.245	0.140	Gazeas et al. (2006)
KIC 9453192*	0.71884	0.099 (0.155)	T	2.314	2.734	1.01	0.438 (0.620)	0.238	0.145	Şenavci et al. (2016); Zola et al. (2017)
XX Sex	0.54011	0.1	SP	1.301	1.87	0.696	0.476	0.236	0.177	Deb & Singh (2011)
UCAC4 479–113711	0.35292	0.1	T	1.400	1.47	0.58	0.893	0.204	0.119	El-Sadek et al. (2019)
NW Aps	1.06556	0.1	T				0.446	0.237		Wadhwa (2005)
AW CrB*	0.36094	0.101	T				0.750	0.244		Broens (2013)
KIC 9350889*	0.72595	0.102 (0.106)	T	2.322	2.775	1.068	0.631 (0.870)	0.234	0.144	Şenavci et al. (2016); Zola et al. (2017)
ASAS J165139+2255.7*	0.35321	0.103	T	1.030	1.27	0.46	0.600	0.216	0.291	Alton (2018)
DN Boo	0.44757	0.103	SP	1.428	1.71	0.67	0.644	0.234	0.127	Şenavci et al. (2008)
FG Hya	0.32783	0.104	SP	1.445	1.438	0.515	0.698	0.244	0.134	Zola et al. (2010)
KIC 10229723*	0.62872	0.105 (0.145)	T	2.110	2.363	0.852	0.023 (0.35)	0.213	0.126	Şenavci et al. (2016); Zola et al. (2017)
ASAS J082243+1927.0	0.28000	0.106	T	1.100	1.15	0.42	0.719	0.225	0.266	Kandulapati, Devarapalli & Pasagada (2015)
GR Vir	0.34697	0.106	SP	1.376	1.49	0.55	0.932	0.232	0.167	Gazeas et al. (2005)
V1191 Cyg*	0.31339	0.107	SP	1.283	1.292	0.503	0.577	0.221	0.184	Ostdadnezhad, Delband & Hasanzadeh (2014)
ASAS J025115–2525.4	0.55927	0.107	T	1.680	2.07	0.7	0.092	0.203	0.115	Saygan (2016)
KIC 7601767*	0.48673	0.107	T	1.784	1.925	0.74	0.449	0.219	0.125	Şenavci et al. (2016)
CK Boo	0.35515	0.111	SP	1.584	1.533	0.65	0.946	0.221	0.125	Deb & Singh (2011)
TYC 6995–813-1 (n)	0.38318	0.111	T	1.230	1.46	0.6	0.720	0.243	0.223	Wadhwa et al. (2021a)
V1222 Tau*	0.29173	0.112	T	0.900	1.06	0.42	0.532	0.209	0.349	Liu et al. (2015)
NSVS 3198272	0.35228	0.115	T	1.621	1.479	0.583	0.391	0.198	0.111	Kjurkchieva et al. (2019b)
KIC 6118779*	0.36425	0.117	T	1.465	1.512	0.657	0.922	0.209	0.118	Şenavci et al. (2016)
V2787 Ori	0.81098	0.12	T	1.440	2.45	0.96	0.181	0.186	0.102	Tian, Zhu & Wang (2019)
AL Lep	0.44864	0.12	T				0.627	0.199		Wadhwa (2005)
KIC 10395609*	0.36425	0.121	T	1.460	1.504	0.657	0.916	0.167	0.093	Şenavci et al. (2016)
Cl* NGC 6121 SAW V66	0.26997	0.123	T	1.660	1.24	0.5	0.322	0.184	0.105	Liu, Qian & Fernández-Lajús (2011)
KIC 10618253*	0.43740	0.125	SP	1.476	1.703	0.756	0.930	0.195	0.111	Şenavci et al. (2016)
$\epsilon$ CrA	0.59143	0.128	SP	1.700	2.1	0.85	0.268	0.175	0.101	Yang et al. (2005a)
KIC 12055014	0.49991	0.128 (0.16)	T	1.781	1.939	0.819	0.597 (0.670)	0.182	0.107	Şenavci et al. (2016); Zola et al. (2017)
V776 Cas	0.44042	0.13	SP	1.550	1.71	0.73	0.646	0.180	0.103	Zhou et al. (2016b)
ASAS J102556+2049.3	0.28498	0.131	T	0.710	1.06	0.39	0.240	0.207	0.456	Kjurkchieva et al. (2019b)
V902 Sgr	0.29394	0.132	T	1.400	1.234	0.513	0.389	0.172	0.096	Samec & Corbin (2002)
ASAS J050334–2521.9	0.41406	0.133	T	1.260	1.54	0.6	0.535	0.171	0.146	Gezer & Bozkurt (2016)
KIC 8265951*	0.77996	0.134 (0.154)	T	2.364	2.816	1.175	0.365 (0.380)	0.143	0.107	Şenavci et al. (2016); Zola et al. (2017)
ASAS J040633–4729.4	0.40637	0.136	T	1.330	1.54	0.6	0.324	0.164	0.127	Saygan (2016)
DZ Psc*	0.36613	0.136	SP	1.370	1.46	0.67	0.987	0.179	0.129	Yang et al. (2013)
HV Aqr	0.37450	0.14	SP	1.240	1.456	0.601	0.740	0.175	0.163	Gazeas et al. (2021a)
HV Aqr	0.37446	0.145	SP	1.355	1.448	0.648	0.568	0.159	0.118	Li & Qian (2013a)
ASAS J142124+1813.1 (n)	0.24300	0.14	T	2.730	1.43	0.57	0.230	0.177	0.118	Kjurkchieva et al. (2019b)
V677 Cen	0.32500	0.142	T				0.341	0.158		Barone et al. (1993)
V710 Mon	0.40520	0.143	T	1.140	1.46	0.66	0.627	0.166	0.189	Liu et al. (2014b)
V410 Aur*	0.36636	0.144	SP	1.270	1.37	0.59	0.290	0.154	0.136	Luo et al. (2017)
HN UMa	0.38260	0.145	SP	1.279	1.42	0.61	0.285	0.153	0.132	Oh et al. (2007)
KIC 9776718 (n)	0.5444	0.146	T	4.880	2.9	1.32	0.915	0.165	0.139	Li et al. (2020)
GSC 1042–2191	0.42380	0.146	T	1.260	1.54	0.69	0.650	0.161	0.146	Bulut, Bulut & Demircan (2016)
NSVS 1917038	0.31807	0.146	T				0.037	0.147		Guo et al. (2020)
KIC 2159783*	0.37388	0.147	T	1.451	1.496	0.694	0.800	0.162	0.095	Şenavci et al. (2016)
XY LMi*	0.43689	0.148	T				0.741	0.159		Qian et al. (2011)
EM Psc	0.34396	0.149	T				0.953	0.163		Qian et al. (2008)
ASAS J113031–0101.9 (n)	0.27100	0.15	T				0.500	0.153		Pribulla, Vanko & Hambalek (2009)
TYC 4157–0683-1	0.39607	0.15	T	1.367	1.499	0.667	0.763	0.157	0.115	Acerbi, Barani & Martignoni (2014)
Mis V1395	0.73930	0.15	T				0.869	0.160		Guo et al. (2020)
V1179 Her (n)	0.38551	0.153	T	1.300			0.450	0.151	0.112	Broens (2021)
V1511 Her (n)	0.35008	0.154	T				0.480			Broens (2021)
ASAS J063546+1928.6	0.47553	0.154	T	1.230	1.184	0.19	0.571	0.149	0.144	Sriram et al. (2018)
AH Cnc	0.36046	0.156	T	1.188	1.332	0.592	0.510	0.144	0.151	Peng et al. (2016)
NGC 6397 V8	0.27124	0.159	T	0.876	0.995	0.456	0.461	0.141	0.248	Li & Qian (2013c)
KIC 3104113*	0.84679	0.159 (0.167)	T	2.440	3.085	1.538	0.947 (0.910)	0.152	0.105	Şenavci et al. (2016); Zola et al. (2017)
Cl* NGC 6715 SAW V144	0.72159	0.16	T	1.310	2.23	0.95	0.195	0.135	0.111	Li & Qian (2013b)
NSVS 1926064	0.40747	0.16	T	1.558	1.605	0.755	0.708	0.146	0.089	Kjurkchieva, Popov & Petrov (2020b)

**Table A1** – *continued*

Name	Period (d)	$q$	Type	$M_1$ ( $M_\odot$ )	$R_1$ ( $R_\odot$ )	$R_2$ ( $R_\odot$ )	$f$	$\frac{f_s}{f_0}$	$\left(\frac{f_s}{f_0}\right)_k$	Reference	
EF Dra	0.42403	0.16	SP	1.815	1.702	0.777	0.467	0.140	0.087	Yang (2012)	
V902 Cep	0.32870	0.162	T	1.077	1.208	0.563	0.470	0.139	0.178	Kjurkchieva et al. (2019b)	
NSVS 2256852	0.34888	0.162	T	0.950	1.18	0.52	0.170	0.134	0.210	Kjurkchieva et al. (2019b)	
V1695 Aql	0.41283	0.162	T	–	–	–	0.831	0.147	–	Samec et al. (2017)	
V972 Her	0.44309	0.164	SP	0.910	1.35	0.59	0.01	0.129	0.215	Selam et al. (2018)	
V1115 Cas	0.32329	0.164	T	1.049	1.181	0.548	0.424	0.137	0.184	Kjurkchieva et al. (2019b)	
GSC 03517–00663	0.29502	0.164	T	–	–	–	0.692	0.142	–	Guo et al. (2015)	
Cl* NGC 104 WSB V95	0.27890	0.165	T	0.970	1.05	0.49	0.743	0.138	0.212	Liu, Qian & Fernández Lajús (2014a)	
AH Aur	0.49411	0.165	SP	1.674	1.897	0.837	0.750	0.149	0.092	Gazeas et al. (2005)	
TV Mus	0.44568	0.166	SP	1.350	1.7	0.83	0.742	0.141	0.110	Qian et al. (2005a)	
V445 Cep	0.44878	0.167	SP	–	–	–	0.517	0.123	–	Oh, Kim & Sung (2010)	
EPIC 211957146*	0.35502	0.17	T	1.050	1.1	0.23	0.642	0.136	0.183	Sriram et al. (2017)	
V345 Gem	0.27477	0.171	SP	1.371	1.134	0.486	0.11	0.128	0.0092	Gazeas et al. (2021a)	
NSVS 13602901 (n)	0.52389	0.171	T	1.190	1.69	0.79	0.440	0.131	0.138	Wadhwa et al. (2021a)	
V1542 Aql	0.41754	0.171	T	–	–	–	0.555	0.113	–	Wadhwa (2004)	
TYC 1337–1137-1 (n)*	0.47550	0.172	T	1.386	1.7	0.83	0.760	0.138	0.100	Liao et al. (2017)	
AS CrB*	0.38066	0.172	T	1.250	1.4	0.67	0.592	0.133	0.126	Liu et al. (2017)	
II UMa	0.82522	0.172	SP	1.990	2.8	2.41	0.869	0.139	0.092	Zhou et al. (2016a)	
OU Ser	0.29677	0.173	SP	1.187	1.155	0.544	0.667	0.129	0.137	Deb & Singh (2011)	
ASAS J002821–1453.3	0.40266	0.173	T	1.330	1.49	0.6	0.397	0.132	0.102	Gezer & Bozkurt (2016)	
KIC 5439790*	0.79609	0.174 (0.192)	T	2.314	2.764	1.29	0.296 (0.360)	0.126	0.085	Şenavci et al. (2016); Zola et al. (2017)	
KIC 8496820*	0.43697	0.176	T	1.566	1.655	0.803	0.596	0.130	0.081	Şenavci et al. (2016)	
PZ UMa	0.26267	0.178	T	0.770	0.92	0.43	0.396	0.124	0.257	Zhou & Soonthornthum (2019)	
V728 Her	0.47129	0.178	SP	1.800	1.87	0.82	0.810	0.111	0.072	Erkan & Ulaş (2016)	
CSS J075258.0+382035	0.42991	0.178	T	1.040	1.44	0.7	0.628	0.130	0.070	Kjurkchieva et al. (2019b)	
GSC 3599–2569	0.40291	0.18	T	–	–	–	0.247	0.119	–	Gorda, Lyaptsev & Sobolev (2015)	
TYC 3700–1384 (n)	0.40747	0.182	T	1.450	–	–	0.490	–	–	Broens (2021)	
GSC 4778–152	0.51746	0.182	T	–	–	–	0.304	0.119	–	Tuvikene et al. (2008)	
TY Pup (n)	0.81920	0.184	T	1.650	2.636	1.373	0.843	0.129	0.084	Sarotsakulchai et al. (2018)	
CN Hyi	0.45611	0.184	SP	1.370	1.6	0.77	0.420	0.120	0.074	Özkardeş, Erdem & Bakış (2009)	
V2388 Oph (n)	0.80230	0.186	SP	1.800	2.6	1.3	0.650	0.123	0.081	Yakut, Kalomeni & İbanoglu (2004)	
GV Leo	0.26673	0.188	T	–	–	–	0.178	0.113	–	Kriwattanawong & Poojon (2013)	
TYC 3836–0854-1 (n)	0.41557	0.19	T	1.200	1.46	0.75	0.794	0.125	0.134	Liao et al. (2017)	
BO Ari*	0.31819	0.19	SP	0.995	1.09	0.515	0.494	0.118	0.176	Gürol, Gürsoytrak & Bradstreet (2015)	
	0.31819	0.207	SP	1.095	1.19	0.636	0.757	0.113	0.147	Poro et al. (2021)	
V619 Peg	0.38872	0.19	T	2.020	1.642	0.811	0.521	0.118	0.079	Kjurkchieva et al. (2019b)	
HV UMa	0.35539	0.19	SP	2.800	2.62	1.18	0.770	0.107	0.077	Csák et al. (2000)	
V1853 Ori	0.38300	0.19	T	1.200	1.36	0.66	0.333	0.114	0.121	He et al. (2019)	
IK Per	0.67603	0.191	T	1.990	2.4	1.15	0.521	0.118	0.079	Zhu et al. (2005)	
Y Sex	0.48774	0.195	SP	1.471	1.568	0.795	0.596	0.117	0.075	Deb & Singh (2011)	
VW Vul	0.38451	0.195	T	–	–	–	0.403	0.112	–	Capezzali, Fiorucci & Spogli (2008)	
EX Leo	0.40860	0.2	SP	1.573	1.56	0.734	0.366	0.112	0.071	Zola et al. (2010)	
V402 Aur	0.60350	0.2	SP	1.638	1.997	0.915	0.031	0.103	0.066	Zola et al. (2004)	
KIC 5809868	0.43939	0.201	T	–	–	–	0.470	0.112	–	Zola et al. (2017)	
NSVS 9045055	0.35459	0.202	T	1.990	1.51	0.751	0.302	0.108	0.073	Kjurkchieva et al. (2019b)	
EL Aqr	0.48141	0.203	SP	1.570	1.73	0.87	0.440	0.109	0.071	Wadhwa & Zealey (2004)	
NSVS 7328383	0.27208	0.205	T	1.013	1	0.49	0.171	0.104	0.151	Kjurkchieva, Popov & Petrov (2019a)	
DN Aur	0.61689	0.205	T	–	–	–	0.468	0.108	–	Godfrey, Leung & Schmidt (1996)	
UY UMa	0.37602	0.206	T	1.151	1.342	0.696	0.606	0.112	0.131	Kim et al. (2019)	
HI Pup	0.43257	0.206	SP	1.210	1.44	0.67	0.203	0.103	0.108	Ulaş & Ulusoy (2014)	
TYC 3836–0854-1*	0.41556	0.206	T	1.383	1.5	0.763	0.592	0.110	0.085	Acerbi et al. (2014)	
ASAS J212236+0657.3	0.29395	0.207	T	0.807	0.793	0.665	0.132	0.102	0.200	Kjurkchieva et al. (2020a)	
TZ Boo*	0.29716	0.207	SP	0.990	1.08	0.56	0.531	0.108	0.165	Christopoulou, Parageorgiou & Chrysopoulos (2011)	
TYC 2402–0643-1 (n)	0.39943	0.208	T	0.860	1.22	0.67	0.220	0.103	0.188	Samec, Caton & Faulkner (2020)	
NSVS 6859986	0.38357	0.208	T	1.870	1.63	0.84	0.860	0.115	0.078	Kjurkchieva et al. (2019b)	
GSC 03950–00707 (n)	0.41200	0.21	T	2.850	1.85	0.91	0.120	0.100	0.076	Kjurkchieva et al. (2019b)	
GM Dra	0.33875	0.21	SP	1.213	1.252	0.606	0.230	0.105	0.110	Gazeas et al. (2005)	
CV Cyg	0.98343	0.21	T	1.600	–	–	0.490	0.108	0.072	Vinko, Hegedus & Hendry (1996)	
RR Cen	0.60569	0.21	SP	1.820	2.1	1.05	0.351	0.104	0.070	Yang et al. (2005a)	
MM Com (n)	0.30199	0.215	T	0.790	0.99	0.35	0.240	0.095	0.184	Kjurkchieva et al. (2019b)	
V409 Hya	0.47227	0.216	T	1.500	1.69	0.9	0.606	0.106	0.071	Na et al. (2014)	
V816 Cep	0.31141	0.219	T	2.830	1.576	0.836	0.511	0.103	0.080	Kjurkchieva et al. (2019b)	
MW Pav*	0.79499	0.22	SP	1.514	2.412	1.277	0.693	0.105	0.070	Alvarez et al. (2015)	
V604 Car	0.47229	0.22	T	–	–	–	0.380	0.101	–	Wadhwa (2006)	
PY Boo	0.27805	0.222	T	0.790	0.93	0.47	0.180	0.096	0.195	Kjurkchieva et al. (2019b)	
FN Cam	0.67713	0.222	SP	2.400	2.61	1.44	0.880	0.110	0.084	Pribulla et al. (2002)	
NSVS 7051868	0.51760	0.223	T	1.610	1.8	0.94	0.353	0.097	0.066	Barani, Martignoni & Acerbi (2017)	
AQ Psc	0.47561	0.226	SP	1.661	1.708	0.891	0.350	0.095	0.065	Deb & Singh (2011)	
V921 Her	0.87738	0.226	SP	1.784	2.56	1.29	0.190	0.090	0.061	Zhou et al. (2016c)	
V921 Her	0.87738	0.244	SP	2.068	2.752	1.407	0.230	0.088	0.061	Gazeas et al. (2006)	
KIC 9832227	0.45796	0.228	SP	1.395	1.581	0.83	0.430	0.096	0.074	Molnar et al. (2017)	
1SWASP J000437.82+033301.2	0.26150	0.23	T	0.820	0.89	0.46	0.116	0.091	0.177	Latković & Čekić (2021)	
(n)	V2357 Oph	0.41557	0.231	SP	1.160	1.386	0.705	0.322	0.093	0.109	Deb & Singh (2011)
ASAS J035020–8017.4	0.62240	0.232	T	0.990	1.76	0.87	0.344	0.094	0.144	Saygan (2016)	
YY CrB	0.37656	0.232	SP	1.393	1.385	0.692	0.228	0.091	0.070	Gazeas et al. (2005)	
YY CrB	0.37656	0.243	SP	1.430	1.43	0.81	0.634	0.104	0.098	Vafiko et al. (2004)	
TYC 5532–1333-1	0.47449	0.232	T	1.510	1.67	0.9	0.343	0.095	0.065	Devarapalli et al. (2020)	
GSC 0763–0572	0.42640	0.233	T	1.230	1.434	0.757	0.310	0.092	0.097	Wang et al. (2012)	

**Table A1** – *continued*

Name	Period (d)	$q$	Type	$M_1$ ( $M_\odot$ )	$R_1$ ( $R_\odot$ )	$R_2$ ( $R_\odot$ )	$f$	$\frac{J_s}{J_0}$	$\left(\frac{J_s}{J_0}\right)_k$	Reference
DU Boo	1.05589	0.234	SP	2.080	3.19	1.74	0.502	0.082	0.060	Djurašević et al. (2013)
V1094 Cas	0.51400	0.235	T				0.300	0.093		Wadhwa (2019)
V789 Her	0.32004	0.236	T	1.130	1.15	0.62	0.238	0.091	0.114	Li et al. (2018)
V2741 Cyg	0.31600	0.236	T				0.480	0.096		Wadhwa (2019)
NSVS 4803568 (n)	0.28657	0.238	T	0.790	0.93	0.43	0.090	0.086	0.172	Kjurkchieva et al. (2019b)
FO Hya	0.46956	0.238	T	1.310	1.62	0.91	0.689	0.098	0.091	Prasad et al. (2013)
GSC 3208–1986	0.40466	0.24	T				0.390	0.092		Samec et al. (2015)
KIC 10267044	0.43004	0.24	T				0.550	0.097		Zola et al. (2017)
V507 Lyr	0.36691	0.24	T				0.200	0.089		Wetterer et al. (2004)
HR Boo	0.31597	0.241	T	1.210	1.17	0.62	0.180	0.090	0.098	Kjurkchieva et al. (2019b)
V404 Peg	0.41918	0.243	SP	1.175	1.346	0.71	0.321	0.089	0.103	Gürol et al. (2011)
GSC 0804–0118	0.32369	0.243	T				0.200	0.087		Yang et al. (2005b)
KIC 3221207	0.47383	0.244	T	1.300	1.67	0.87	0.790	0.096	0.090	Aliçavuş & Soydugan (2017)
T-Dra0-00959 (n)	0.32933	0.245	T	0.890	1.06	0.5	0.240	0.084	0.147	Kjurkchieva et al. (2019b)
UW CVn	0.29247	0.245	T				0.202	0.086		Kopacki & Pigulski (1995)
TYC 01963–0488-1	0.42704	0.248	T	1.370	1.46	0.78	0.347	0.088	0.073	Alton (2016)
HI Dra	0.59742	0.25	SP	0.720	1.98	1.08	0.240	0.085	0.061	Papageorgiou & Christopoulou (2015)
KN Per	0.86650	0.25	T				0.545	0.090		Yang & Qian (2015)

This paper has been typeset from a T<sub>E</sub>X/L<sup>A</sup>T<sub>E</sub>X file prepared by the author.